



**TORSIONAL FRETTING WEAR
EXPERIMENTAL ANALYSIS OF A R3
OFFSHORE STEEL AGAINST A
PC/ABS BLEND**

THIAGO PANDIM BARBOSA MACHADO

**DISSERTAÇÃO DE MESTRADO EM CIÊNCIAS MECÂNICAS
DEPARTAMENTO DE ENGENHARIA MECÂNICA**

FACULDADE DE TECNOLOGIA

UNIVERSIDADE DE BRASÍLIA

**UNIVERSIDADE DE BRASÍLIA
FACULDADE DE TECNOLOGIA
DEPARTAMENTO DE ENGENHARIA MECÂNICA**

**TORSIONAL FRETTING WEAR
EXPERIMENTAL ANALYSIS OF A R3
OFFSHORE STEEL AGAINST A
PC/ABS BLEND**

THIAGO PANDIM BARBOSA MACHADO

Orientador: PROF. DR. THIAGO DOCA, ENM/UNB

DISSERTAÇÃO DE MESTRADO EM CIÊNCIAS MECÂNICAS

**PUBLICAÇÃO PCMEC.DM - XXX/AAAA
BRASÍLIA-DF, 22 DE NOVEMBRO DE 2019.**

**UNIVERSIDADE DE BRASÍLIA
FACULDADE DE TECNOLOGIA
DEPARTAMENTO DE ENGENHARIA MECÂNICA**

**TORSIONAL FRETTING WEAR
EXPERIMENTAL ANALYSIS OF A R3
OFFSHORE STEEL AGAINST A
PC/ABS BLEND**

THIAGO PANDIM BARBOSA MACHADO

DISSERTAÇÃO DE MESTRADO SUBMETIDA AO DEPARTAMENTO DE ENGENHARIA MECÂNICA DA FACULDADE DE TECNOLOGIA DA UNIVERSIDADE DE BRASÍLIA COMO PARTE DOS REQUISITOS NECESSÁRIOS PARA A OBTENÇÃO DO GRAU DE MESTRE EM CIÊNCIAS MECÂNICAS

APROVADA POR:

Prof. Dr. Thiago Doca, ENM/UnB
Orientador

Prof. Dr. Cosme Roberto Moreira da Silva, ENM/UnB
Examinador interno

Prof. Dr. Michel Sullivan Teixeira Pires, IFG
Examinador externo

BRASÍLIA, 22 DE NOVEMBRO DE 2019.

FICHA CATALOGRÁFICA

THIAGO PANDIM BARBOSA MACHADO

TORSIONAL FRETTING WEAR EXPERIMENTAL ANALYSIS OF A R3 OFFSHORE STEEL AGAINST A PC/ABS BLEND

2019xv, 74p., 201x297 mm

(PCMEC/FT/UnB, Mestre, Ciências Mecânicas, 2019)

Dissertação de Mestrado - Universidade de Brasília

Faculdade de Tecnologia - Departamento de Engenharia Mecânica

REFERÊNCIA BIBLIOGRÁFICA

THIAGO PANDIM BARBOSA MACHADO (2019) TORSIONAL FRETTING WEAR EXPERIMENTAL ANALYSIS OF A R3 OFFSHORE STEEL AGAINST A PC/ABS BLEND. Dissertação de Mestrado em Ciências Mecânicas, Publicação xxx/AAAA, Departamento de Engenharia Mecânica, Universidade de Brasília, Brasília, DF, 74p.

CESSÃO DE DIREITOS

AUTOR: Thiago Pandim Barbosa Machado

TÍTULO: TORSIONAL FRETTING WEAR EXPERIMENTAL ANALYSIS OF A R3 OFFSHORE STEEL AGAINST A PC/ABS BLEND.

GRAU: Mestre ANO: 2019

É concedida à Universidade de Brasília permissão para reproduzir cópias desta dissertação de mestrado em Ciências Mecânicas e para emprestar ou vender tais cópias somente para propósitos acadêmicos e científicos. O autor se reserva a outros direitos de publicação e nenhuma parte desta dissertação de mestrado pode ser reproduzida sem a autorização por escrito do autor.

Thiago Pandim Barbosa Machado

Campus Darcy Ribeiro, Asa Norte. Faculdade de Tecnologia, Departamento de Engenharia Mecânica

Acknowledgements

First of all, I would like to thank my beloved wife Janaína, for all the support given throughout this hard journey that has been the Master's course. She, better than anyone, knows the effort invested in this work, and has always motivated me to continue this pursuit, even in the most challenging moments. During the last two years, she has been of enormous emotional help, and has also abdicated from a lot, in order for me to focus on this research. Without her help, none of this would have been possible. For that and for the daily love and effort she puts in me and in our family, I will be forever grateful. Thank you, my love.

Special thanks are also due to my parents, Ricardo and Rosangela. Throughout my whole life, they have always supported me in all possible meanings of the word. Many times, when demotivated and doubting this choice of pursuing a Master's degree, they were the ones who put me back on track and did everything in their power so I wouldn't have to worry about anything but this course. One day I shall be able to repay all their effort and I hope to be a great of a parent to my son as they are to me. Until then, all I can say is thank you, mom and dad.

Another very important person in this journey was my mother-in-law, Neusa. She has also gone out of her way to help me through these years, spending her vacations and free time helping me and my wife with our son, so I could focus on this work. Thank you very much, Neusa.

I would also like to thank my supervisor, Prof. Thiago Doca. More than a professor, he played a crucial role as a mentor and a model to be followed. Always pushing me to go forward and expand on my research, Prof. Doca really acted as a great supervisor and explored my potential.

Last, but certainly not least, I would like to mention my son, Lucas. Since he was born, he has always been the reason for everything in my life. It was no different regarding this course. The countless hours I had to stay away from him shall be repaid in the near future. One day you will read this, my son, and hopefully you will understand that this effort was ultimately done to provide a better future to our family. Thank you for being the single most important thing in my life, Lucas.

To my beloved son, Lucas.

Resumo

Sistemas de ancoragem, normalmente usados em embarcações de Unidades Flutuantes de Produção, Armazenamento e Transferência (FPSO, na sigla em inglês) são compostos de correntes metálicas acopladas a cabos de poliéster. É sabido que a falha de até mesmo uma única corrente pode ter consequências catastróficas, desde poluição ambiental até a perda de vidas. Muitas causas de falhas prematuras dessas correntes foram identificadas, sendo o desgaste por *fretting* uma muito importante. Esse tipo de desgaste ocorre na região entre os elos, que realizam movimento torsional alternante. O foco deste estudo é determinar a aptidão de uma mistura específica de polímeros, a saber, Policarbonato/Acrilonitrila-Butadieno-Estireno (PC/ABS) com uma razão mássica de 60:40, para revestir elos de correntes de ancoragem feitos de aço *offshore* de grau R3.

Para alcançar esse objetivo, ensaios experimentais foram feitos na configuração esfera-plano com dois pares de materiais: R3 X PC/ABS 60:40 e R3 X R3 (chamada de condição de referência). Foram feitos ensaios com cargas normais de 1.0 kN e 2.0 kN, para 0, 50, 100 e 200 milhares de ciclos com uma faixa de $\pm 1.0^\circ$ a 5 Hz. As marcas de desgaste foram analisadas com um microscópio confocal a laser.

As amostras de PC/ABS exibiram taxas de desgaste muito maiores do que as de aço R3. Entretanto, o polímero também apresentou um comportamento notavelmente previsível, ao que o aço R3 exibiu uma evolução de desgaste altamente não linear com o aumento do número de ciclos. Com base na previsibilidade mostrada pelo PC/ABS, pode ser estimado que um revestimento de 5 mm de espessura dessa composição de polímeros poderia estender a vida de um elo de corrente de ancoragem em 25.4 milhões de ciclos a 1.0 kN e em 4.6 milhões de ciclos a 2.0 kN.

Dados os resultados, conclui-se que o PC/ABS 60:40 pode, de fato, levar a um aumento significativo na vida dos componentes e na confiabilidade de um sistema de ancoragem.

Abstract

Mooring chain systems, mainly used in Floating Production Storage and Off-loading (FPSO) vessels are composed of metallic chains coupled with polyester cables. It is known that the failure of even one of those chains can have catastrophic consequences, ranging from environmental pollution to loss of lives. Many causes of early failure of those chains have been identified, fretting wear being a very important one. This type of wear occurs in between links, which exhibit torsional reciprocating motion. This study focuses on determining the suitability of a specific polymer blend, i.e. Polycarbonate/Acrylonitrile-Butadiene-Styrene (PC/ABS) with a 60:40 weight ratio, to coat a R3-graded offshore steel mooring chain link.

To accomplish that, experimental testing was done in a sphere-to-flat configuration with two material pairings: R3 x PC/ABS 60:40 and R3 x R3 (called the reference condition). Tests were made with 1.0 kN and 2.0 kN normal loads, for 0, 50, 100 and 200 kcycles of $\pm 1.0^\circ$ range at 5 Hz. Wear scars were analyzed with a confocal laser microscope.

The PC/ABS samples showed much higher wear rates than R3 steel. However, the former also exhibited a remarkably predictable behavior, whereas R3 displayed a highly non-linear evolution of wear with increasing number of cycles. From that predictable behavior, it can be estimated that a 5 mm thick coating of this polymer blend could extend the lifetime of a mooring chain link by 25.4 M cycles at 1.0 kN and by 4.6 M cycles at 2.0 kN.

Given the results, it is concluded that PC/ABS 60:40 could indeed lead to a significant increase in component lifetime and reliability of a mooring system.

SUMMARY

1	INTRODUCTION	1
1.1	MOTIVATION AND THE STATE OF THE ART.....	1
1.2	OBJECTIVES	6
1.3	OUTLINE	6
2	THEORETICAL BACKGROUND.....	8
2.1	CONTACT MECHANICS.....	8
2.1.1	FRICITION	9
2.1.2	CONTACT BETWEEN SOLIDS AND HERTZ THEORY	14
2.2	WEAR	18
2.2.1	ADHESIVE WEAR	20
2.2.2	ABRASIVE WEAR	21
2.2.3	FATIGUE WEAR	22
2.2.4	CORROSIVE WEAR	23
2.2.5	FRETTING WEAR	24
2.3	MICROSCOPY ANALYSIS AND WEAR VOLUME ESTIMATIONS	27
3	MATERIALS AND METHODS.....	29
3.1	EXPERIMENTAL SETUP.....	29
3.2	MATERIALS	30
3.3	TEST PROGRAM	31
3.4	EXPERIMENTAL PROCEDURES	32
3.4.1	PREPARATION OF THE SAMPLES	32
3.4.2	PURE COMPRESSION PHASE	33
3.4.3	TORSIONAL FRETTING WEAR TESTS	33
3.4.4	MICROSCOPY ANALYSIS	34
4	RESULTS AND DISCUSSIONS.....	40
4.1	HARDNESS OF THE MATERIALS	40
4.2	SCAR MORPHOLOGY	41
4.3	WEAR ANALYSIS	45
4.4	LIFE ESTIMATIONS	50

5 CONCLUSIONS	52
REFERENCES	54

LIST OF FIGURES

1.1	Schematic representation of a general load scenario found in mooring chains. (a) Forces due to masses, currents, waves and buoyancy; (b) Displacements and rotations.	2
1.2	Mooring line system for an FPSO [1]	5
2.1	Cuneiform characters for mineral oil products and animal fat. Extracted from [2].	10
2.2	Depiction of a Egyptian statue being moved on a wooden sledge. Extracted from [3].	11
2.3	Two non-conforming surfaces interacting at point O. Reproduced from [4].	15
2.4	Interference fringes generated by the contact of two equal cylindrical lenses with their axes inclined at 45° a) unloaded ; b) loaded. Reproduced from [4]. .	16
2.5	Cross section of two non-conforming surfaces touching. Reproduced from [4].	17
2.6	Comparison between stress distributions at the contact surface and along the z-axis: a) caused by uniform pressure, b) caused by Hertz pressure. Reproduced from [4].	18
2.7	Descriptive terms of wear and their interrelations. Reproduced from [5].	19
2.8	Schematics of the four principal wear modes. Reproduced from [5]).	20
2.9	Four simple fretting modes for sphere-to-flat configuration: a) Tangential Fretting, b) Radial Fretting, c) Rotational Fretting, d) Torsional Fretting. Reproduced from [6].	25
2.10	Typical optical morphology of radial fretting scar for a dental ceramics. Extracted from [6].	25
2.11	Evolution of wear scars of rotational fretting for LZ50 steel, normal load of 10 N and angular range of $\pm 0.25^\circ$. Extracted from [6].	26
2.12	Scar morphology of torsional fretting wear for 7075 steel alloy, with normal load of 100 N, angular displacement of $\pm 0.5^\circ$ and 5,000 cycles. Extracted from [6].	26
3.1	Depiction of representative specimens of each test configuration.	30
3.2	Holding device (version 1.1 [7]) used for the flat specimens.	31

3.3	Experimental setup for the wear tests. Machine used: MTS 809 Axial-Torsional. (a) Equipment: 1) Crosshead, 2) Force transducer, 3) Top cell, 4) Upper grip, 5) Lower grip, 6) Bottom cell. (b) Detailed view of the specimens: 7) Hemispherical pad, 8) Flat sample, 9) Holding device.....	36
3.4	Olympus LEXT OLS4100 confocal laser microscope.....	37
3.5	Carl Zeiss AXIO Imager M2 optical microscope. Extracted from manufacturer's catalog.....	37
3.6	Illustration of the contact configuration, restraints and loading conditions used. (a) Encastre on the hemispherical pad (red area) and lateral face constraint (orange area); (b) normal load and z-axis rotation.....	38
3.7	Computer-aided volume measurement method. Applied only to R3 samples. ..	38
3.8	Representative 3D (top) and 2D (bottom) profiles of flat samples used for quantifying the wear volume, by measuring the scar's depth and diameter. (a) PC/ABS 60:40 ; (b) R3 steel.	39
4.1	Two dimensional profiles of the R3 steel flat counterparts and hemispherical tools' tips.	42
4.2	Two dimensional profiles of the PC/ABS 60:40 flat counterparts.	43
4.3	Detailed view of the chipping patterns on the tip of a hemispherical tool. Test conditions: R3 x R3, 1.0 kN, 200,000 cycles.	44
4.4	Three dimensional profiles of the R3 steel samples. Test conditions: 1.0 kN, 200,000 cycles.....	46
4.5	Net wear volume versus number of cycles: reference configuration (R3 x R3).	47
4.6	Net wear volume versus number of cycles: PC/ABS 60:40 flat counterpart.	49
4.7	Wear depth versus number of cycles: PC/ABS 60:40 flat counterpart.....	49

LIST OF TABLES

3.1	Mechanical properties of the R3 offshore grade steel and the PC/ABS 60:40 blend.	30
3.2	Wear tests program matrix	32
4.1	Hardness of the flat counterparts.....	40
4.2	Volume measurements: reference configuration.	47
4.3	Volume estimations: PC/ABS 60:40 flat counterpart.	48
5.1	Examples of limits set up on the Limit Detector.	59

Chapter 1

Introduction

1.1 Motivation and the State of the Art

Floating Production Storage and Off-loading (FPSO) vessels are often employed for the exploration of oil and gas. The mooring system, used to attach such vessels to the sea floor, is typically composed of 8 to 12 mooring lines. Each line has a metallic chain on the dry section and several polyester cables below the water level. The failure of even one of those lines can result in structural damage, loss of lives and environmental issues. Those consequences range from production stoppage for mechanical repairs to severe oil spills onto the oceans [8, 9, 1]. Failures of mooring chains may happen for a number of reasons and on different parts of the structure. The most common parts for failure are the chain links located in the vicinity of fairleads, connectors and wire ropes [9, 1]. Moreover, besides the usual failure mechanisms of chains on such applications, it has been noted that other novel failure mechanisms play an important role, such as out-of-plane bending, pitting corrosion and chain twisting [10].

Wear, in particular the fretting wear that occurs between chain links, is regarded as an important factor in chain failures, since it reduces significantly the strength of mooring lines and promotes the development of cracks [9, 11]. That is true not only for mooring systems, but also for different types of situations as well. Shackel chains employed in fishing nets, for example, are submitted to circular and planar motions which often cause abrasive wear [12], whereas loads commonly applied in mooring systems chains [13, 14] promotes the development of fretting wear [15] when relative angular motion exceeds 0.5° [16]. A thorough review of this topic was done by Waterhouse [15]. Among his findings, it is important to highlight that extremely small slip amplitudes and frequencies can produce appreciable damage, and that oxidation processes in the fretting of steels at room temperature might play a major role in the evolution of the wear damage. A typical metallic section of a mooring system chain, composed of chain links and D-type connectors, can be seen in Fig. 1.1, along with possible forces, rotations and displacements experienced by the system.

It is safe to say that the traction required to restrain a FPSO is significant. In the design

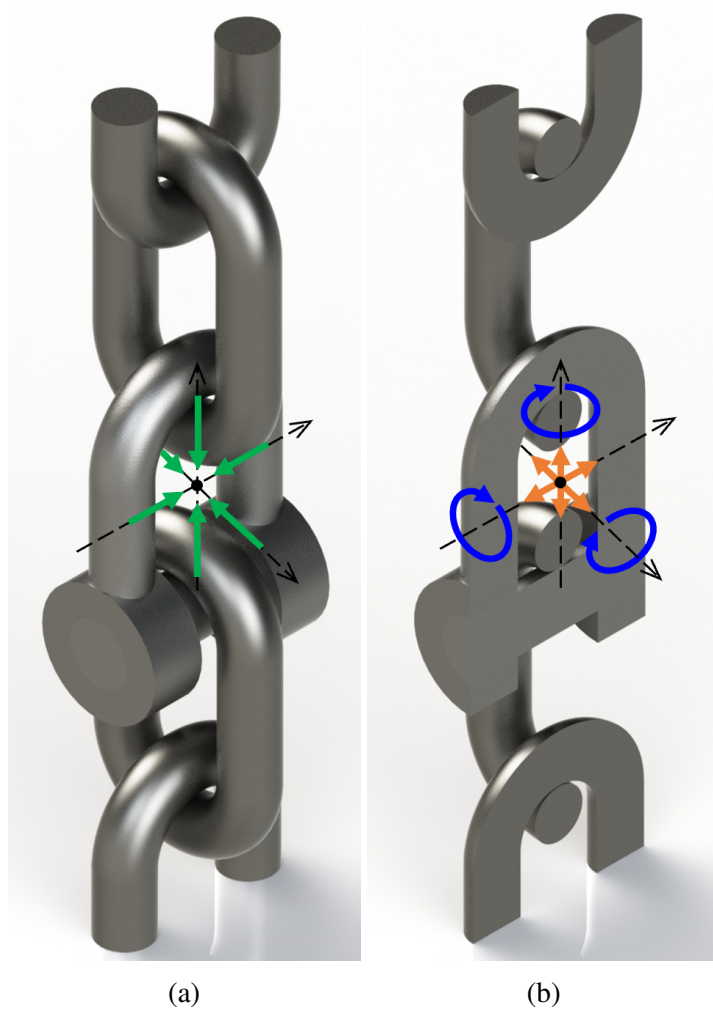


Figure 1.1: Schematic representation of a general load scenario found in mooring chains. (a) Forces due to masses, currents, waves and buoyancy; (b) Displacements and rotations.

stage of such systems, the concept of Minimum Breaking Load (MBL) is used to determine the number of lines, the dimensions of chain links and the materials to be employed. Depending on the steel grade chosen, the load on a standard 120D offshore chain link may reach up to 70% of its MBL [17]. The normal contact forces, at this load level, result in plastic strains that flatten the contact interface, inhibiting some of the motions produced by tides, waves and water currents. Given the variety of components employed in a mooring line, each one with different shapes and in contact with various elements (chain links, bolts, connectors, squared pins, etc.), different contact configurations can be found in a mooring line. However, given the relatively small areas that are actually in contact, these configurations usually can be fairly approximated by crossed-cylinders, cylinder-to-flat or sphere-to-flat, with appropriate equivalent radii. Evidently, each separate component can exhibit six degrees of freedom, i.e., given a $\{x, y, z\}$ rectangular coordinate system, it can rotate around and move along each axis. Nevertheless, in ultra deep mooring systems, the tensile loads applied on the chains (in the z-direction) are so high one can state that only z-axis rotation, i.e., torsion, is able to produce enough relative motion to promote wear [18], while restraining the remaining degrees of freedom. Furthermore, assuming that the traction on the system is up

to the standards, one can expect both an adhesion zone and a mixed-slip zone (where small amplitude, reciprocating motion occurs) to be formed. Therefore, under these conditions, a torsional fretting wear condition is attained.

Some alternatives have been proposed to mitigate wear phenomena on chain links. Elastic chains have been suggested as alternative for the metal ones. These chains would be manufactured by burying steel chain links within a rubber column, so that the elastic properties of the rubber would reduce wear and the impulsive tension acting on the chain. Simulations have been done with such a design and have shown up to a 50% reduction in the impulsive tension [19]. Mooring line systems, with different dynamic behavior, are also under analysis [20]. Another possibility would be to coat the contact zone of the critical chain links with a soft yet resistant material (e.g. polymers or elastomers). This could reduce wear and, therefore, prevent failures of mooring line systems or, at least, provide predictable data to designers and maintenance engineers, avoiding unexpected failures.

Polymer blends are known for their interesting tribological properties. For instance, Polycarbonate/Acrylonitrile-Butadiene-Styrene (PC/ABS) is a polymer blend widely used in the automotive and consumer electronics industries due to its availability, good impact resistance, high strength modulus and high thermal stability [21, 22, 23]. Its popularity can be explained by the nearly additive nature of the blend's properties with respect to its components [24, 25]. A blend with a higher concentration of PC with respect to ABS has the tendency to be less flexible, more difficult to machine and have higher overall mechanical strength. On the other hand, a blend with a higher percentage of ABS should be easier to machine and have higher impact resistance and toughness.

A study on the friction and wear behavior of 18 polymers fretted against steel in dry air and humid environments can be found in [26]. It was observed that the addition of fillers in a polymer matrix has different effects on the wear rate depending on the environmental conditions. Zaitsev [27] investigated the contact of a cobalt and tungsten carbide alloy against a number of polymers and their composites. He concluded that the predominant wear mechanism depended on the chemical composition of the polymer. More specifically, he discovered that for polymers containing active oxygen groups, the most relevant wear mechanism was based on oxidation-fatigue. When in contact with polymer composites, the alloy would show wear marks compatible with abrasive wear. The more general conclusion of his work was that the type of wear depends on the polymer's (or composite's) ability to form friction transfer layers (FTL) on the metallic surface. Therefore, an adequate choice for the PC/ABS ratio could provide a suitable coating for the chain links of a mooring system.

The effects of parameters such as surface hardness, surface topology and contact geometry on fretting wear rates have also been studied. Lemm et. al. ([28]) conducted experimental tests to understand the role of surface hardness on the debris retention in the fretting wear of steel pairs. Namely, the specimens were made of the same AISI Type 01 steel, but with different surface hardness obtained by heat treatments, and the contact configuration was cylinder-on-flat. It was shown that for pairs of specimens with the same hardness, the fretting

wear volume had a relatively small variation as the hardness was increased. For specimens of different hardness, a variation of 30% in the wear volume for the pairs with the highest differential of hardness as compared to the equal hardness pairs was found. Moreover, there was a significant difference in the distribution of wear between the two specimens in the cases with different hardness. It was observed that when the difference in hardness reaches a critical value, the oxide-based fretting wear debris were preferentially retained, resulting in a protection of the softer specimen and preferential wear of the harder specimen. However, when low frequencies were applied, the wear on the softer specimen was greatly accelerated, which was linked to a reduction in the ability of the debris to be effectively retained within the fretting contact.

Another factor that seems to have a great influence in fretting wear mechanisms is the frequency. Kirk et al. [29] conducted fretting wear experiments using high strength steels in the cylinder-on-flat configuration across a range of frequencies. They observed that, for higher frequencies, the wear damage was lower than for lower ones. Considering that in the contact between metallic materials, oxidation processes, and more specifically, the formation of oxide-based debris is a major source of potential damage, it would be reasonable to think that higher frequencies would result in higher damage, since the higher temperature in the contact region would promote and accelerate oxidation. While that is also true, the decrease in damage with higher frequencies observed by the researches was attributed to the less time available for the oxides to grow. Besides, it was proposed that these higher temperatures would promote changes to the bulk material properties, fostering sub-surface plastic deformation during the fretting process, which would account for more damage.

Coatings have distinct surface properties that enhance the mechanical performance of its substrate. They are often hard, resilient, thermal-protective and non-conductive. In moving parts, coatings also have low coefficients of friction and wear. The assessment of such surface properties is commonly carried out using a traditional tribometer in unidirectional linear motion. Usually, the contact geometry is not considered relevant for the purposes of testing, since it is argued that the wear phenomenon depends only on the true area of contact, generated by micro asperities on the surfaces of the materials in contact, which is assumed to be proportional to the normal load. By that reasoning, regardless the initial contact configuration, after the true contact area is established, the wear mechanism would evolve the same way it would with any other initial geometry. However, Warmuth et al. [30] has shown experimentally that fretting wear can, indeed, be geometry-dependent. They observed that for less-conforming contact configurations, the dominant wear mechanism results in damage by bulk material removal, while for more conforming contacts, damage caused by subsurface deformation and adhesive transfer is dominant. They argue that, despite the friction coefficient being independent from contact geometry, the wear coefficient, at least for fretting displacement amplitudes, is indeed dependent on the initial configuration. This happens not because of the changes in contact pressure, but rather due to the debris flowing out or being retained within the contact zone.

A torsional fretting wear condition is achieved when an adhesion zone and a mixed-slip zone are formed at the interface of solids under a reciprocate angular motion of small amplitude. The literature regarding this topic, specially concerning the interaction between polymers and metals, is relatively poor, despite the fact that torsional wear happens in many mechanical and biological systems, such as human hip and knee joints and controllable pitch propellers. Zhang et al. [31] did experimental comparisons between torsional fretting wear and sliding wear of CuNiAl against 42CrMo4. The data revealed that, due to solid lubrication effects of debris and strain hardening of the worn surfaces, the fretting wear rate was lower than the sliding wear rate. Moreover, they showed that oxidation, cracks and delamination are the dominant wear mechanisms for fretting tests.

Many works have investigated both the failure mechanisms of mooring chain systems (see [1], [32], [9]) and the thermal and mechanical properties of PC/ABS blends (see [21], [22], [23]). However, few attention has been given to the wear resistance of this polymer and its possible applications, such as coating for the metallic chains in mooring systems, in order to possibly provide better wear resistance and prevent premature failures.

Given the clear importance of the topic and considering the lack of research on this particular area, an analysis of the torsional fretting wear behavior of the R3-Offshore steel and a Polycarbonate/Acrylonitrile-Butadiene-Styrene (PC/ABS) blend is presented. The goal of this study is to identify the surface properties (i.e. hardness and wear rate), wear morphology and quantify a possible life extension of a chain link due to a PC/ABS coating.

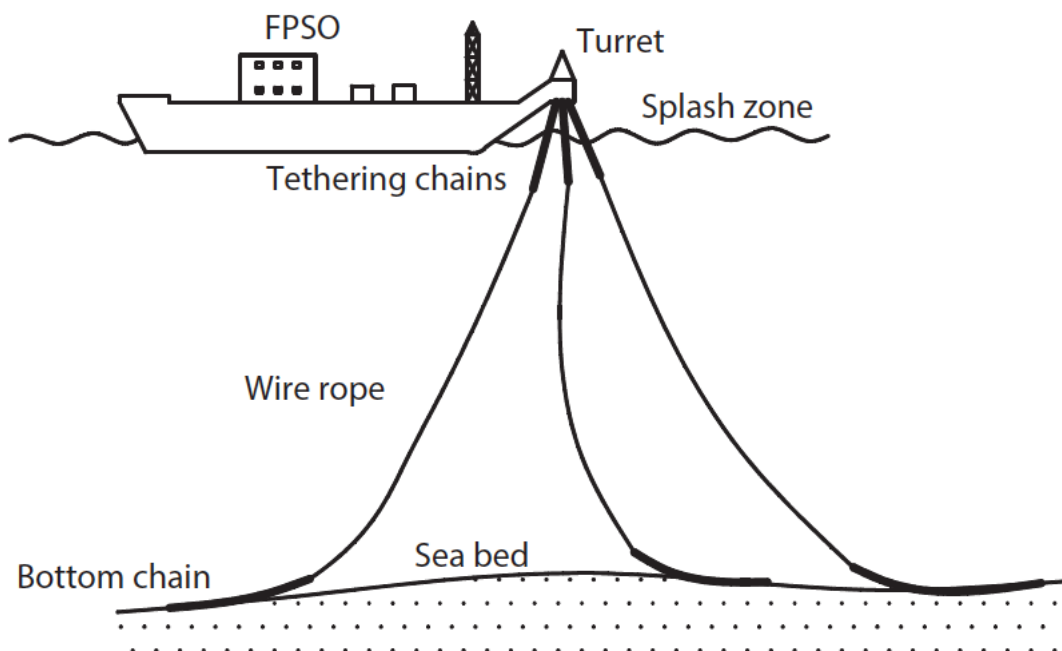


Figure 1.2: Mooring line system for an FPSO [1]

1.2 Objectives

The main objective of this work is to analyze and evaluate a particular blend of PC/ABS with a 60:40 weight ratio of PC to ABS as a possible candidate for coating of metallic chain links used in mooring systems. In order to accomplish that, other objectives can be listed as follows:

- Evaluate surface properties of this specific polymer blend, such as hardness;
- Calculate the wear rate of this polymer under cyclic torsional fretting load applied by a tool made of R3 graded offshore steel, and compare those to a reference condition, namely, R3 x R3;
- Estimate a possible life extension for a chain link coated with this specific polymer blend;
- Determine in a conclusive way if PC/ABS 60:40 is a suitable and viable candidate for coating R3 steel chain links in mooring systems

1.3 Outline

This work is structured in six chapters as follows:

Chapter 2

In this chapter, a literature review regarding the most relevant theories to this work is presented. In particular, the following topics are explored in different:

- Contact Mechanics this section presents a comprehensive review of the development of friction models is given in a chronological way. It starts with the first evidences of humankind exploring the resistance to motion in their favor, and goes all the way to modern friction theories. Then, the development of contact theories is briefly explained, focusing on the notorious Hertz Theory of Elastic Contact.
- Wear: covers all the relevant topics concerning perhaps the most important phenomenon studied in this work, i.e. wear. The basic concepts of wear are briefly presented, along with its different types. Finally, the most relevant type of wear for this work, i.e. fretting wear is explored in more detail;
- Wear volume estimations and microscopy analysis: a brief review of microscopy methods used to inspect wear marks is presented, along with both traditional and novel methods for evaluating wear volume and wear rate for different fretting wear modes.

Chapter 3

The materials and methodology used to accomplish the objectives of this work are presented in this chapter. In particular, the mechanical tests run to obtain the relevant data are described along with the test matrix and the microscopy analysis.

Chapter 4

In this chapter, the results attained from the experimental testing are comprehensively presented and discussions are made based on the data analysis.

Chapter 5

The final part of the work presents a summary of the most relevant conclusions made from the data analysis in the preceding chapter. Moreover, some recommendations are made for future works on the same topic.

Chapter 2

Theoretical Background

In this chapter, an overview of the theoretical aspects of the more relevant topics for this work is given. The first part contains a historical background is presented by chronologically summarizing the study of friction from its initial stages to the current theories. It is followed by a brief description of the problem of contact between two solids, and Hertz Theory of Elasticity is described in more detail, since it is the most used one for analytical solutions even in present times. The second part focuses on the different types of wear are presented and some specific considerations regarding fretting wear. The third and final part of the chapter regards microscopy techniques and different methods used to evaluate wear damage.

2.1 Contact Mechanics

Contact Mechanics, as the name implies, is the study of the motion of bodies that interact with each other at one or more points. Aside from the obvious occurrences of physical contact in human daily life, from walking to operating a computer, the physics of contact plays a tremendous role in industrial applications. The design of even the most usual machine element, e.g. gears and bearings, must consider the effects of the contact it will have with its surroundings. More complex systems and entire machines must also be designed considering the contact between its parts and between the machine and its surroundings. Even though all these applications involve contact mechanics, different tasks concerning this area may be of more relevance to each particular case. Many times one will try and minimize the friction between two bodies, as it will dissipate energy and may decrease the machine's efficiency. Focus on this case might be on the lubrication of the part or the optimization of its geometry. In other instances one might be interested on the stress analysis of an element under a determined load condition. A third situation might involve the study of contact between micro components on a computer chip, which will consider different characteristics and behaviors. The fact is that contact mechanics permeates many different branches of the physical and engineering sciences and is of the outermost importance.

Were that not enough reason to explore this topic, its economical impacts are also profound. The very name of the area that studies friction, wear and lubrication (all of which are contact phenomena), i.e. tribology, arises from a report on the problems of these phenomena and their economical impacts on industry [33]. In this report, the cost of issues related to the aforementioned phenomena is emphasized and savings about 1.0% to 1.4% of the Gross Domestic Product - GDP could be reached by implementing better tribological practices, based on studies carried out in several industrial countries. Given the importance of this topic, Prof. Jost suggested that a new scientific concept should be formulated to generalize all the aspects of the interactions and relative motions between solids. The term tribology (from the greek *tribos*, meaning rubbing) was then coined as *the science and technology of interacting surfaces in relative motion and of related subjects and practices* [34]. More recently, the losses connected to friction and wear are estimated to be around 3% to 5% of the GDP of industrial countries. Moreover, approximately 25% of the energy input in industry is spent on overcoming friction forces. [34, 35].

Keeping in mind the relevance and importance of the matter above described, a chronological review of the developments in contact mechanics is presented in the next section.

2.1.1 Friction

Humans have dealt with contact problems and friction phenomena for thousands of years. Even in prehistoric times, before 3,500 B.C., the ancient man used the resistance to motion in his favor. Perhaps the earliest examples of that are the invention of fire, accomplished by rubbing dry wood and generating heat and the invention of the wheel, using rolling friction to move an object with less effort. The earliest records of people using materials such as oil, bitumen and fat go back to the Sumerians, the first known civilization in Mesopotamia, and can be found in their cuneiform characters (see Fig. 2.1), which could mean they used such materials as lubricants in rudimentary systems. However, a much clearer example of a device used to facilitate the transport of large structures can be seen in Fig. 2.2 (from around 2,400 B.C.), where a person is depicted pouring a substance in front of a wooden sledge, while several others pull the statue. That is evident knowledge of lubrication and how to take advantage of the different friction coefficients of materials.

Moving forward a few thousand years to late 15th and early 16th centuries, Leonardo Da Vinci's notes on mechanics show the first persistent effort to understand the characteristics of friction in a systematic manner. Even though the earliest record of his insights on the matter is a 92mm X 63mm piece of paper found only many centuries later (see [36] for more details), it was on his Codex-Madrid I from 1485 [37] that his conclusions were more clearly stated. Having done several experiments with solid blocks of different shapes and sizes on inclined and horizontal planes, Da Vinci's findings can be summarized as follows:

1. The frictional force between two sliding surfaces is proportional to applied normal;

Sumeric	Akkadic	German	English
	samnum	Öl, Fett	oil, fat
	ittu, kupru	Bitumen, Erdpech (ursprünglich „Quelle“)	bitumen, pitch
	šaman itti	Öl von Bitumen	oil from bitumen
	kupru	Asphalt, Mastix	asphalt, mastix
	ittu ellu, ittu namru	Glänzendes Bitumen	shining asphalt
	ittu šadi	Bergasphalt	mining asphalt
	šaman šadi	Öl aus dem Berge	mining oil
	ittu me heru	Bitumen aus dem Wasser	bitumen from water
	ittu isati, ittu šaripu	Feuerbitumen, brennendes Bitumen	fire or burning bitumen
	apsû	Bitumen-Abgrund (Süßwasserquelle)	bitumen-abyss (fresh water spring)
	nabātu - naptu	leuchten - Naphta	shining - naphta

Figure 2.1: Cuneiform characters for mineral oil products and animal fat. Extracted from [2].

2. The frictional force does not depend on the contact surface area;

Those are known today as the two fundamental laws of friction developed by Da Vinci. He was also the first to name the proportionality constant in the first law as *coefficient of friction* and, based on his experiments, he stated that its value is generally equal to 0.25.

However, he realized that different materials sliding on the same surface present different levels of difficulty to move, which shows some insight on the variation of coefficient of friction depending on the material analyzed. Moreover, he made notes about the increase and decrease of this coefficient based on surface roughness and the presence of a third material (e.g. lubricants or other solids), which he stated as: *...different bodies have different kinds of friction; because if there shall be two bodies with different surfaces, that is that one is delicate and smooth and well-greased or soaped, and it is moved upon a plane of a similar nature, it will move much more easily than one that has been roughened by the use of file or rasp and ...rough and hard with rough and hard – movement of the greatest difficulty; rough and soft with rough and soft – medium difficulty.* Leonardo Da Vinci continued to give contributions regarding tribology, as he developed many experiments involving various types of friction [36].

Despite the fact that Da Vinci's findings were of great importance, some would argue that they had no significant impact on the engineering of the time. In 1699, the first widely discussed document regarding the study of friction was written. It was Guillaume Amon-

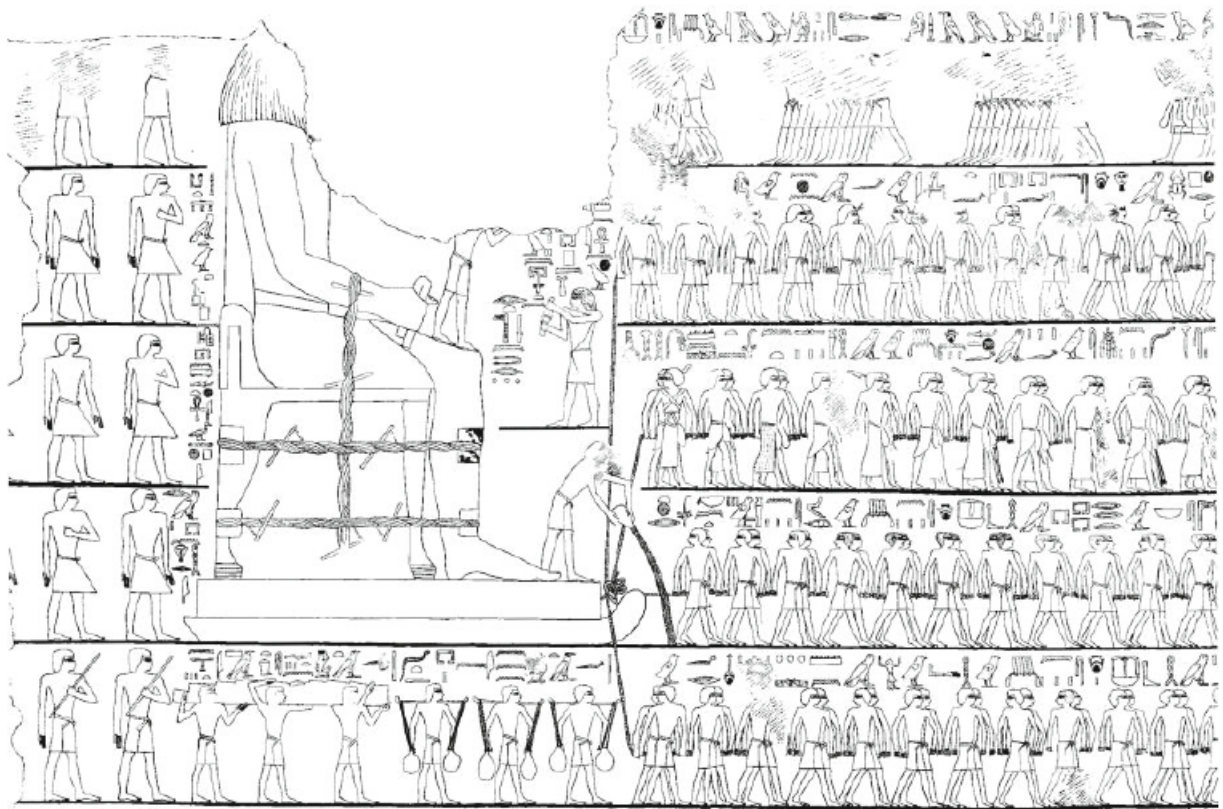


Figure 2.2: Depiction of a Egyptian statue being moved on a wooden sledge. Extracted from [3].

ton's memoirs, whose most notable feature was to simplify the complex phenomenon of dry friction. He stated four laws of friction, as follows:

1. The resistance caused by friction increases/decreases in proportion to pressure;
2. The resistance caused by friction is the same for iron, copper, lead and wood as long as they are lubricated with a grease;
3. This resistance is roughly equal to one-third of pressure;
4. This resistance does not depend on velocity and other conditions.

This very rough depiction of nature was not supported by rigorous mathematical theories. Nevertheless, it did summarize a not well-understood phenomenon at the time, with relatively good insight for practical applications. His works had such a great impact on the physics and engineering that the proportionality of friction to the normal force applied on an object is called Amontons's law [38].

A substantially more complete and rigorous work on the matter was later done by Charles Augustin Coulomb, whose contributions to distinct fields, such as electromagnetism, friction and mechanics gave him, besides scientific prizes, the timeless fame of a true scientist. For detailed descriptions of his works, the reader is referred to [38] and [39]. Following

a purely experimental procedure, apparently not connected to any robust theoretical background, Coulomb did extensive studies on the dependency between friction and several factors with different material couples. The relations explored by him can be summarized as follows:

1. Dependence of the sliding friction force on the normal force: Coulomb presented extensive data on the inverse coefficient of friction, i.e., the ratio between normal and frictional forces. He found that this ratio varied depending on the material couple, but usually showed a strong relationship between both forces;
2. Dependence of the static force of friction on the contact time: It was already known that the static coefficient of friction depends on the contact time between the surfaces. For that reason, Coulomb's notes would never show a single value for this coefficient, but rather values for different time intervals, such as 0.5 s, 2 s, 10 s and 1 h. The fact that there was a very large gap between the last two time instants is evidence that he observed the friction force to become stable after a few seconds and not change from that point on;
3. Dependence of the force of friction on the contact size: Amontons had already stated the weak relationship between the friction force and contact area. Coulomb confirmed that, but, because of the much more rigorous and large set of experiments, he also found that, in some cases, there was a significant dependence between the friction force and the contact area.
4. Dependence of other parameters: Coulomb tried to summarize the influences of other parameters in two-term equations, such as Eq. (2.1), where τ is the tangential stress in a given plane of a material point, τ_0 is the tangential strength at zero normal stress and σ_N is the normal stress in the given direction and μ is the "internal" coefficient of friction. Generally, these equations would involve a first term with large contribution to the variable in question second relatively weak term.

$$\tau = \tau_0 + \mu\sigma_N \quad (2.1)$$

The so-called *Coulomb's Law of Friction*, i.e., *the frictional force is independent of the contact area and velocity and it is proportional to the normal force*, as it is stated in textbooks, is only a small part of his conclusions regarding friction. His findings about the relation between the force of friction and both the apparent contact size and the normal force can be stated simply as: *for a given frictional pair, the coefficient of friction becomes larger as the indentation depth of the roughness of the two bodies become smaller*. In other words, the indentation depth can be considered the most relevant parameter of the process of friction, as it was corroborated by others (see [40]).

Even though Coulomb's model is still used in simple situations, it does not take into account any energy dissipation mechanism, which should clearly be considered, since fric-

tion is a non-conservative force. A simple yet elegant demonstration of Coulomb's model inconsistency is presented by Hutchings [41].

Between 1930 and 1970, Bowden and Tabor developed the classic model for sliding friction, which states that there are two sources for the friction force, namely adhesion and deformation. The former would account for the microscopic forces between both surfaces at the real contact points, and the latter refers to the deformation action needed to move the asperities over each other. Therefore, each component of this force must have a separate coefficient of friction, which is usually denoted as μ_{adh} and μ_{def} for adhesion and deformation, respectively. A first approximation of this model, considering an idealized sliding contact between two metal surfaces results in predicted values for the adhesion and deformation coefficients of approximately 0.2 and 0.1. However, experimental data does not agree with those approximations. Indeed, measured values of the static coefficient of friction (the sum of both terms, i.e., $\mu_{adh} + \mu_{def}$) are usually much greater than the expected [41].

Two main effects can explain this deviation of data: junction growth and work-hardening. Junction growth refers to the phenomenon where tangential forces, and therefore, tangential stresses, may play a major role in increasing or decreasing the real contact area. Indeed, the model above described assumed that the contact area was determined only by normal loads. However, tangential stresses deform and reshape asperities, so that the real contact area increases with increasing tangential force, and the value of μ also increases proportionally. Moreover, assuming a thin film with shear strength τ_i less than the shear strength of the bulk material τ_o placed on the contact interface, it can be shown that the coefficient of friction is predicted as

$$\mu = \tau_i/p_o \tag{2.2}$$

where p_o is the yielding strength of the bulk material. This equation gives insight to lubrication, since it shows a way to reduce the coefficient of friction by introducing a thin layer of lower shear strength material on the contact interface.

On the other hand, work-hardening refers to the fact that, since all metals strain-harden to some degree, the asperity junctions will considerably work-harden, i.e., their shear strength will increase significantly in comparison to the original indentation hardness of the material. That results in an increase in μ_{adh} . This increase is, however, difficult to quantify precisely.

The Bowden and Tabor model cannot, however, account for all phenomena observed experimentally. Indeed, the assumptions made are not valid for every case. For instance, in practical applications, surfaces can slide on each other with low wear and high friction. Were the plastic deformation of asperities the reason for that dissipation of energy, extremely high wear rates would be required, which are not observed. Therefore, theories are needed which would explain energy dissipation without invoking dislocation motion at the points of contact as the explanation.

Some ideas have been explored in that sense. A possible explanation for some part of the energy dissipation is the elastic waves produced by atoms at the contact interface, vibrating around their equilibrium positions during sliding motion. Those waves, usually called *phonons*, could explain friction in some cases, since they carry energy away from the contact and into the surroundings. But even that could not explain incommensurate interfaces (i.e, the contact between solids with different spacing of surface atoms), since, in those cases, vibration in energy and interaction forces with sliding distance is much less, and could not be a significant contributor to friction.

The origins of friction at microscopic scale are still elusive, as well as quantitative models for predicting macroscopic coefficient of friction between non-lubricated contacts [41].

2.1.2 Contact between solids and Hertz Theory

A very important point of concern when studying contact between solids is the stress distribution and evolution before and during the contact on each surface. This is the motivation behind the so-called contact theories. Heinrich Hertz was the first one to develop a comprehensible and satisfactory analysis of stresses at the contact of two elastic solids. His findings when summarized are called *Hertz Theory of Elastic Contact*, and can be found on his two famous papers, published on 1822, called, in free translation, "*On the contact of elastic solids*" and "*On the contact of elastic solids and on hardness*" [42, 43].

Kenneth Langstreth Johnson (1925 to 2015), a professor of engineering at the University of Cambridge, wrote the book *Contact Mechanics* [4] which would later be regarded as a classic in the area. On this book, he introduces Hertz Theory of Elastic Contact in an elegant yet rigorous manner. The reader is referred to that text for a thorough explanation. Nevertheless, a brief introduction and the most important results of his theories shall be here mentioned.

First, consider a contact between two non-conforming surfaces, as shown in Fig.2.3. As one moves them towards each other, an area of contact begins to appear. First, it is only a point and, as the contact progresses, it becomes an elliptical area. That can be shown both mathematically (see [4], page 85) and experimentally by observing the interference fringes generated between two cylindrical lenses, as seen on Fig. 2.4. In other words, let h be separation distance between the surfaces, R' and R'' the principal curvature radii of the surfaces at the origin of the coordinate system, i.e., the maximum and minimum value of the curvature radius of all possible cross-sections of the profile. Then, it is readily shown that

$$h = \frac{1}{2R'}x^2 + \frac{1}{2R''}y^2 \quad (2.3)$$

proving the elliptical shape of the contact area.

In order to determine a stress distribution, consider a cross section of the contact between both surfaces and analyze their deformation, given a compressive load P , as shown in Fig.2.5.

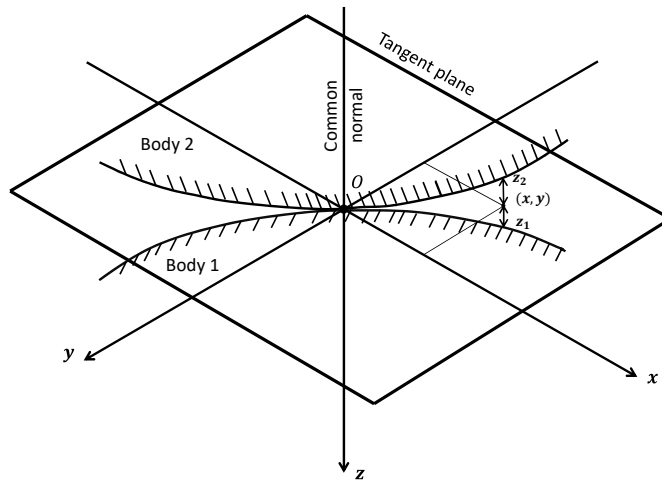


Figure 2.3: Two non-conforming surfaces interacting at point O. Reproduced from [4].

Would the surfaces not deform, their profiles after moving towards each other would overlap, as shown by the dotted lines. Before any deformation occurs, the distance between their surfaces are given by Eq. (2.3). What actually happens is that distant points, such as T_1 and T_2 , move parallel to the z-axis by δ_1 and δ_2 , respectively. Because of the contact pressure, the surface of each body is displaced also parallel to the z-axis by a quantity u_{z1} and u_{z2} , relatively to T_1 and T_2 . After deformation, the contact area might take different shapes, e.g. circle, line, etc. With simple geometric considerations, Johnson shows how the pressure distributions and elastic displacements are obtained for different configurations. By doing a dimensional analysis on this problem, one can promptly find the mean contact pressure p_m which satisfies the aforementioned geometrical assumptions for two touching surfaces of materials with principal radii R_1 and R_2 and elasticity moduli E_1 and E_2 . The result is that, for given material and geometry, the contact pressure and associated stresses rise in direct proportion to the linear dimension of the contact area [4].

In order for Hertz to derive the expressions for pressure and stress distribution precisely for specific cases and, hopefully, for general situations, he considered the same aforementioned situation, as follows. Consider a contact between two surfaces with relative curvature radius R , principal radii R_1 and R_2 and characteristic body dimensions l (both laterally and in depth). Assume that:

1. The surfaces are continuous and non-conforming: $a \ll R$;
2. Deformations are small: $a \ll R$;
3. Each solid can be regarded as an elastic semi-space: $a \ll R_1, R_2$ and $a \ll l$;
4. There is no friction on the surfaces, i.e., the tangential forces q_x and q_y are zero.

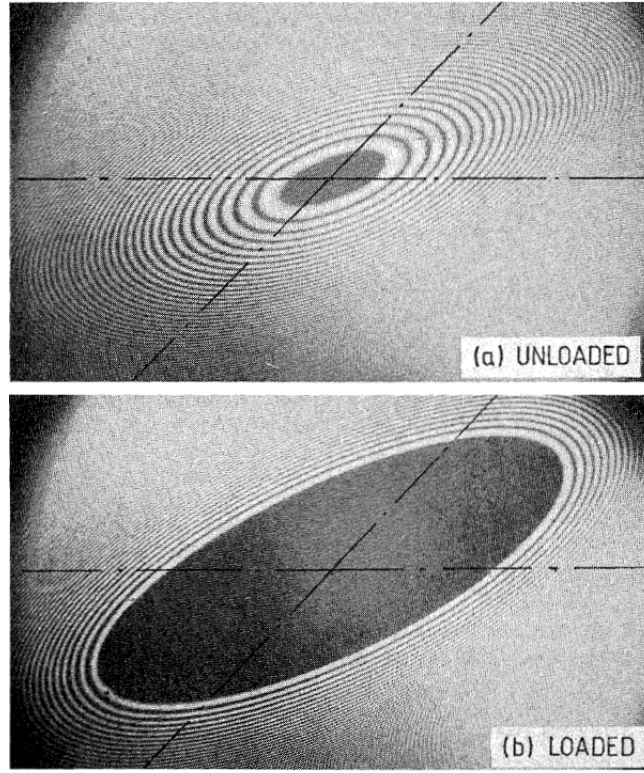


Figure 2.4: Interference fringes generated by the contact of two equal cylindrical lenses with their axes inclined at 45° a) unloaded ; b) loaded. Reproduced from [4].

Applying the theory of elasticity and mechanics of solids known at the time, Hertz was able to derive powerful expressions for some parameters of interest. He found, for instance, that the contact area radius for contact between revolution solids (which generate a circular contact area), a , the displacement of each point on the surface, δ , and the maximum pressure at the interface, p_o , are given, respectively, by

$$a = \left(\frac{3 PR}{4 E_{eq}} \right)^{\frac{1}{3}} \quad (2.4)$$

$$\delta = \frac{a^2}{R} \quad (2.5)$$

$$p_o = \frac{3 P}{2 \pi a^2} \quad (2.6)$$

where E_{eq} is an equivalent strength modulus for both materials, whose value is determined by

$$E_* = \left(\frac{1 - \nu_1^2}{E_1} + \frac{1 - \nu_2^2}{E_2} \right) \quad (2.7)$$

It should be noted that there is an equivalency between a sphere-on-flat and crossed-cylinder contacts in specific cases. Namely, when two cylinders with radii R' and R'' are placed on each other at a right angle, the contact contours are given exactly by Eq. (2.3). In other words, it is possible to obtain identical contact areas and pressure distributions for two completely

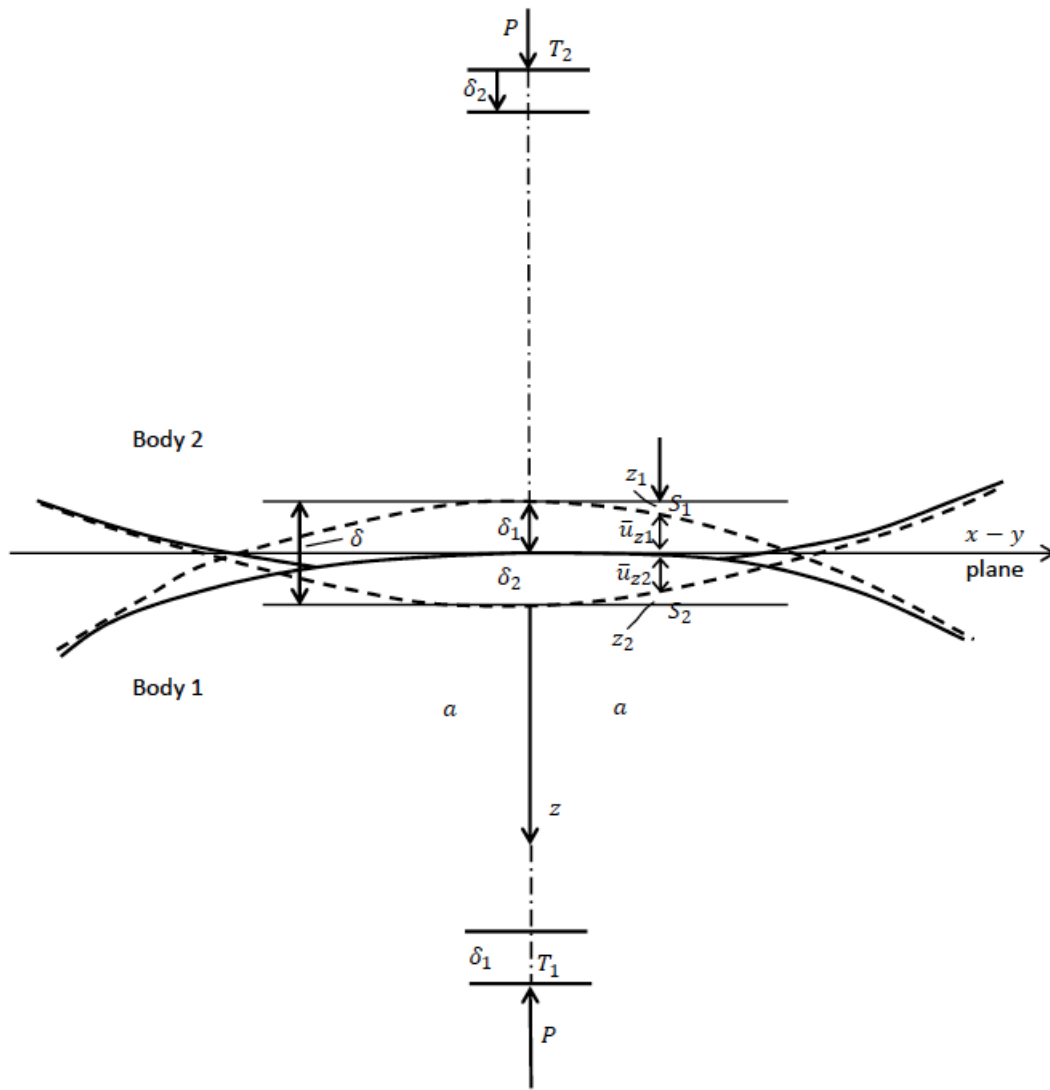


Figure 2.5: Cross section of two non-conforming surfaces touching. Reproduced from [4].

different configurations, by choosing specific equivalent radii.

For illustration purposes, a comparison between the stress distributions caused by uniform pressure and calculated by Hertz's theory is shown in Fig. 2.6

Along the z -axis, σ_r , σ_z and σ_θ are principal stresses. It is important to note that the principal shear stress τ_{max} happens not on the surface, but underneath it, at a fraction of the radius a . Therefore, an important conclusion is that plastic yielding is expected to happen first under the surface, and not on it. Moreover, one can readily see that all stresses are compressive, except at the edges of the contact area, where it is of tensile nature and has its maximum value equal to $(1 - 2\nu)\frac{p_0}{3}$. That is precisely the stress responsible for annular cracks that happen in brittle materials.

It is important, however, to note that Hertz's theory is valid for elastic materials operating within their elastic domain. The equations can be used to predict the behavior of the contact up until the point where plastic yielding starts.

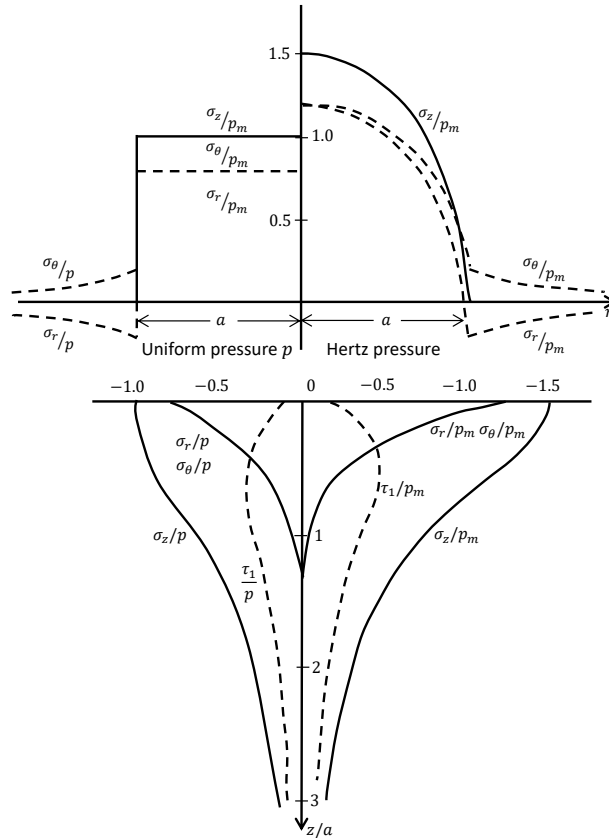


Figure 2.6: Comparison between stress distributions at the contact surface and along the z-axis: a) caused by uniform pressure, b) caused by Hertz pressure. Reproduced from [4].

2.2 Wear

The contact between real solids can involve many mechanisms, some of which have already been described, such as deformation, adhesion, friction and changes in material properties (for instance, work-hardening). Another essential phenomenon present to some degree in almost every contact is wear. Wear can be defined as *the process of gradual removal of material from surfaces of solids subject to contact and sliding* [44]. It can also be understood as *the result of material removal by physical separation or due to microfracture, by dissolution or by melting at the contact interface* [5].

Studies on wear mechanisms go back to 1930, when the scientific community was inclined to believe that friction occurred due to attractive forces between surfaces. Hence, as explained above, came the adhesion theories of the time. This led some authors to develop models which described the loss of material during contact between solids as a consequence of adhesion. Tabor himself theorized that, in the presence of adhesive forces, dissimilar materials would fare during sliding contact. He stated that three situations might happen, depending on the strength of the interface of contact:

1. Interface weaker than both metals: no metal transfer is expect to occur, e.g. tin on steel;

2. Interface stronger than one metal and weaker than the other: metal transfer occurs from the softer material to the harder surface and wear particles - debris - might escape from the system, due to shearing of the softer metal, e.g. lead on steel;
3. Interface stronger than the hardest metal: metal transfer occurs both ways, but mainly from the soft to the hard metal, e.g. copper on steel.

It should be noted, however, that those statements could not be rigorously proved, since the very definition of interface strength does not exist [45]. Being such a broad concept, wear mechanisms have been divided in many different ways and categories, which are not always well defined. Here, the classification given by Kato [5] will be used. Many descriptive terms of wear, according to his classification, are shown in Fig.2.7. Nevertheless, four

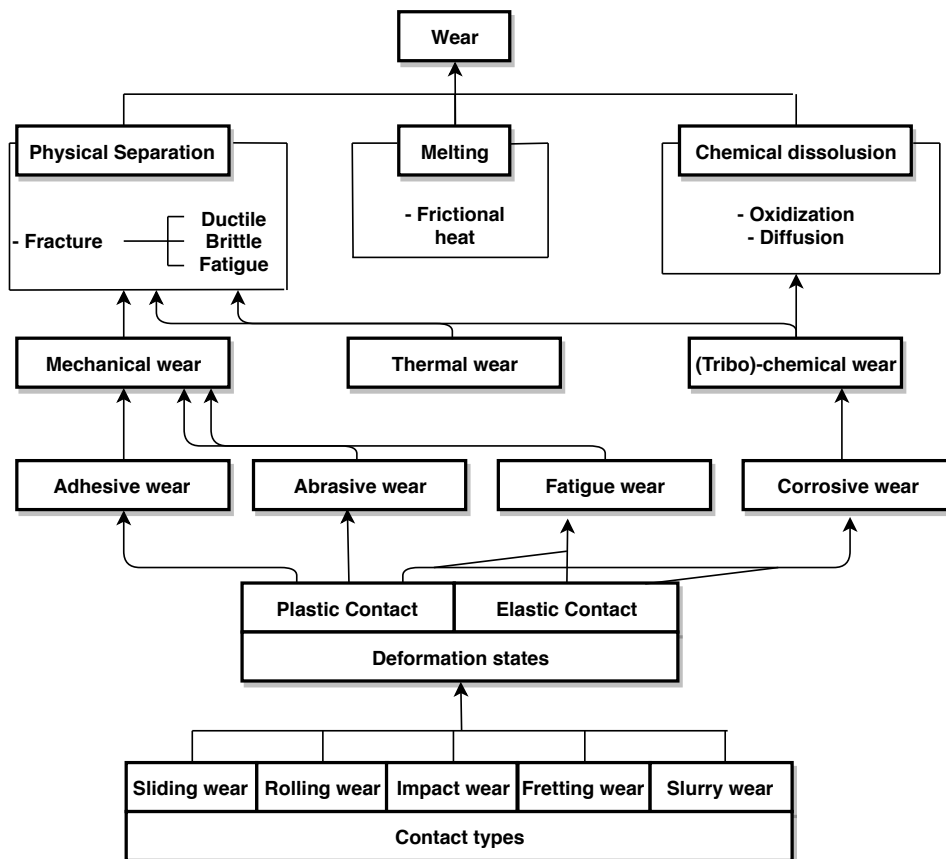


Figure 2.7: Descriptive terms of wear and their interrelations. Reproduced from [5].

wear modes are considered the most important and generalized enough to encompass most practical phenomena. Those are: adhesive wear, abrasive wear, fatigue wear and corrosive wear, as shown schematically in Fig. 2.8. Each one shall be here briefly described, since they are of importance to this work.

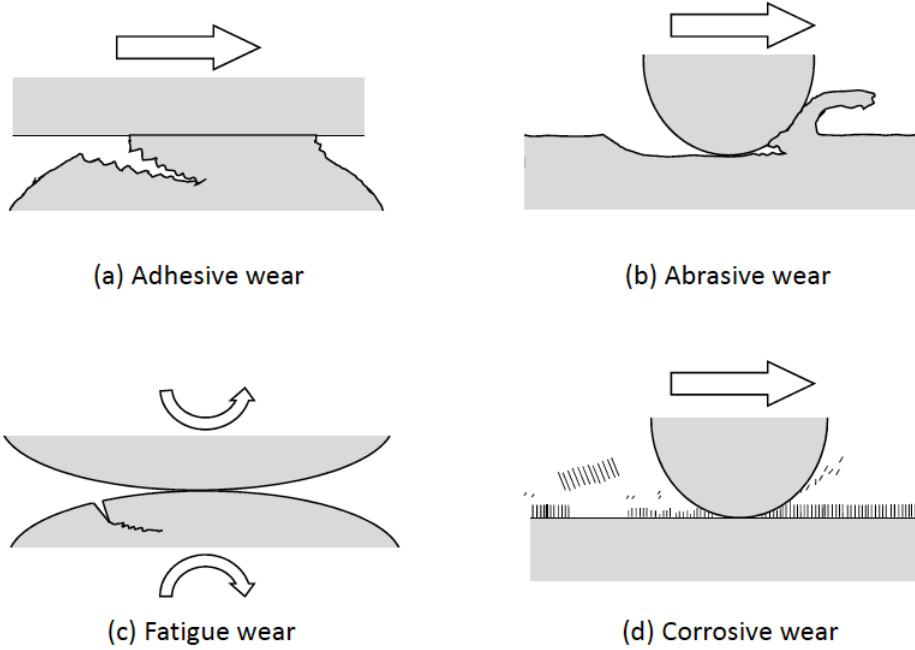


Figure 2.8: Schematics of the four principal wear modes. Reproduced from [5]).

2.2.1 Adhesive Wear

Consider a contact whose interface has a bonding strength such that the resistance to sliding motion is so intense that large plastic deformation is generated in the contact region under shearing and compression. Naturally, that is the case for plastic contact between similar materials, even though dissimilar contacts may also show high bonding forces. This large deformation might result in a crack, which evolves and propagates due to the combined effect of shearing and tensile stresses. When the crack reaches the surface, a wear particle is formed and it is said that adhesion transfer occurred. Archard [46] proposed a method to estimate the volume of material worn during the sliding contact between two solids. In order to do so, he first assumed that the number of points of contact remained constant during the sliding, i.e. if a contact point vanishes, a new one is formed so that the total number is kept the same. Furthermore, he assumed the contact area to be circular of radius a and the normal contact pressure to be nearly equal to the hardness H of the wearing material. Thus, he concluded that the possible wear volume V of a contact between two solids sliding a distance L under a load W is

$$V = \frac{1}{3} \frac{WL}{H} \quad (2.8)$$

However, it was experimentally proved that adhesive wear occurs in many different ways, such that the wear particle size does not always correspond directly to the contact area, as assumed before. Moreover, sometimes the debris would not come from the softer material, but rather from the harder one. In order to take into account all these observations, instead of the factor $\frac{1}{3}$ in Eq. (2.8), a parameter K_{adh} was introduced, which is called wear coefficient for adhesive wear or simply Archard's coefficient. Therefore, the notorious Archard's wear

equation can be written as

$$V = K_{adh} \frac{WL}{H} \quad (2.9)$$

It should be noted that this value is not a constant for a pair of materials, but rather a value which depends on both the material properties and the operation parameters. It usually ranges from 10^{-7} to 10^{-2} [46, 47]. An important conclusion from Eq. (2.9) is that the wear volume is proportional to both the normal load and the sliding distance [5].

2.2.2 Abrasive Wear

This wear mode usually refers to *the scraping or cutting off of superficial particles by particles, edges or other entities that are hard enough to produce more damage to another solid than to itself*. [45]. In order to understand this wear mode, suppose a contact between two surfaces where, during the sliding motion, a interlocking of inclined or sharp edged particles occurs. The work done on that area may result in ploughing, i.e., the removal of material due to abrasive contact. This generates an abrasive groove, usually on the weaker surface. However, for this wear mode, two situations must be differentiated, i.e., abrasive wear of ductile materials and abrasive wear of brittle materials. For ductile materials, because of the deformation ability of the particles, long, ribbon-like wear particles are usually generated during sliding, by the mechanism of microcutting, similar to machining a ductile metal in a lathe. Similarly to adhesive wear, an equation to estimate the wear volume, based on the load, sliding distance and the hardness of the wearing material was derived and is such that

$$V = K_{ab} \frac{WL}{H} \quad (2.10)$$

In Eq. (2.10), the factor K_{ab} is called the coefficient of abrasive wear, whose value ranges typically from 10^{-4} to 10^{-1} for metals [48]. Relative to K_{adh} , K_{ab} usually results in much larger wear volumes. Because of that, abrasive wear is commonly understood as severe wear.

For brittle materials, the analysis should be somewhat different. When ploughing takes place in the contact of brittle materials, the wear particle generated is usually sharp edged and relatively small, when compared to the ones generated in ductile materials. This removed particle results in a crack on the surface of the material, which may propagate and lead to more worn material. Therefore, the abrasive wear resistance of a brittle material is strongly dependent on its fracture toughness. A model for predicting the wear volume in these cases was developed by Evans and Marshall [49], which resulted in the following equation for the predicted wear volume

$$V = \alpha_3 \left(\frac{W^{\frac{9}{8}}}{K_c^{\frac{1}{2}} H^{\frac{5}{8}}} \right) \left(\frac{E}{H} \right)^{\frac{4}{5}} L \quad (2.11)$$

where α_3 is a material-dependent constant, E is the material's Young modulus and K_c is its fracture toughness. Different assumptions lead Evans and Wilshaw [49] to another predictive

equation, as follows

$$V = \alpha_4 \left(\frac{W^{\frac{5}{4}}}{K_c^{\frac{3}{4}} H^{\frac{1}{2}}} \right) L \quad (2.12)$$

Both Eq. (2.11) and Eq. (2.12) agree well with experimental data for brittle metals.

2.2.3 Fatigue Wear

Differently from adhesive and abrasive wear modes, fatigue wear occurs in contacts where material is worn due to a number of contact cycles. Many subcategories can be used in this wear mode, depending on whether the contact is elastic or plastic, whether the damage mechanism is high-cycle fatigue or low-cycle fatigue and whether the sliding amplitude is small (called fretting) or large, among others [45]. For elastic contacts, e.g. rolling elements, the main wear mechanism is high-cycle fatigue fracture in the contact region. Even though the apparent contact pressure is lower than the yielding strength of the material and, therefore, no plastic deformation should occur, local yield does happen in the contact region, due to microdefects of the material. There is even the possibility that a plastic deformation occurs beneath the surface and does not reach it, due to work hardening in the yield region caused by repeated contact.

The whole mechanism can be summarized as follows: the accumulation of plastic strain and stress concentration points caused by repeated sliding in elastic contacts result in cracks after a determined number of cycles. These cracks are propagated in a similar way to fatigue fracture, ending up with removed material by fatigue wear. For plastic contacts, differently from abrasive wear, a wear particle is not removed at the first pass of a hard, perhaps sharp-edged particle over a softer one. Instead, what happens is that, for each pass, only a shallow, conformable groove is formed. After a certain number of cycles, the effect of repeated sliding is such that material is removed [5]. Challen et. al [50] described the predicted wear volume V by considering the plastic work needed to remove a unit volume of material by

$$V = \frac{r_p \mu}{k C_s^D \Delta \gamma_s^{1-D}} W L \quad (2.13)$$

where r_p is the ratio of plastic to total work of sliding, k is the average shear flow stress of the wearing material, $\Delta \gamma_s$ is the effective shear strain increment per pass, D is a constant (usually taken as 2) and C_s is the monotonic effective shear strain. Eq. (2.13) can be rewritten in the form of Eq.(2.9) and Eq. (2.10) (see [45]), so that

$$V = K_f \frac{W L}{H} \quad (2.14)$$

where

$$K_f = \frac{3\sqrt{3} r_p \mu}{C^D \Delta \gamma_s^{1-D}} \quad (2.15)$$

is called fatigue wear coefficient.

2.2.4 Corrosive Wear

When a reciprocating contact is established in a corrosive medium, two possible situations may occur if a considerable reaction takes place between the medium and the materials. The first possibility is that the reaction products strongly adhere to both surfaces and behave like their bulk materials. In this scenario, wear mechanisms are essentially similar to those in non-corrosive media. The second possible outcome, however, happens when the reaction products behave very differently from the bulk material. In this case, wear phenomena is considerably different from that of the bulk material, and is dominated by these new substances formed from the chemical reactions. This last situation is called corrosive wear [45].

The most important mode of corrosive wear of metals is definitely oxidative wear. The oxidative reactions between metals and elements such as oxygen generate films of oxides on the surfaces of metallic bodies, which is then removed in a sliding contact. The removal of such films usually create fine and disperse powders, composed of metallic oxides, which might play different roles in the contact. These debris might act as third bodies in the contact interface, preventing strong adhesion between metallic surfaces. They might also increase abrasive damage, since the oxides formed from a certain metal are usually harder than the original material.

A corrosive wear coefficient K_c can be defined analogously to the other wear modes. Considering the removal of an oxide film formed by the reaction between a steel surface and normal atmospheric air, Quinn [51] proposed that

$$K_c = \frac{LA}{\xi^2 \rho^2 v} \exp\left(-\frac{Q}{R_g T}\right) \quad (2.16)$$

where A is the Arrhenius constant, Q the activation energy, R_g the gas constant, T the absolute temperature, ρ the oxide density, v the sliding velocity and L the distance along which the wearing contact is made.

An important note to be made above Eq. 2.16 is the influence of temperature in the corrosive wear. Indeed, the temperature at the contact interface is essential to understand what type of wear prevails and its intensity, since oxidation is usually promoted more rapidly in higher temperatures. As explained in Sec. 1, many works show the relationship between temperature and corrosive wear. Waterhouse [15], for instance, observed that oxidation processes might play a major role in wear development, even at extremely small amplitudes and room temperature.

This work focuses on the fretting wear of metallic samples against both metallic and polymeric counterparts. The experiments are supposed to emulate the conditions found in the dry-section of mooring chain systems used in FPSO's. Even though the studied part of these chains are above the water level, it should be noted that saline mist, i.e., air with dissolved sea salts, might play an important role in the wear mechanism of the chain links.

However, the experiments presented in this work were not able to account for that, and should be considered of limited validity for highly moist air conditions.

2.2.5 Fretting Wear

Fretting wear is of the outermost importance to this work, and shall be here explained. Fretting refers to relatively small amplitude, high frequency oscillatory slip motion between two solid surfaces in contact [5]. These motions usually range from fractions of micrometers to hundreds of micrometers, and occur daily in many systems, such as in hip joints and bones, gears on shafts, mooring chains, and many others. This small and usually fast oscillation causes debris to form in the interface of the contact and, perhaps more importantly, tends to keep those debris in the contact area, which is the main difference between fretting and large amplitude sliding. Therefore, the removed material can increase future damage or even lubricate the contact, acting as third body.

According to Ludema [45], fretting wear usually begins at a high rate but levels off after 5,000 to 10,000 cycles for steel, depending on the ductility of the oxide. This is important, because the wear debris formed during such contacts are intimately related to the oxide particles generated by the metals. Indeed, even their color and shape change depending on the material properties and operation parameters. At low pressures and temperatures, debris from steel are usually red. Increasing pressure increases compaction of the particles, giving a black color to the removed material. Still according to Ludema [45], the oxygen availability is a major factor to consider when studying the influence of frequency on fretting. That is because the aforementioned red, hexagonal $\alpha\text{Fe}_2\text{O}_3$ usually seen in steel fretting contacts may suffer further oxidation if the conditions allow for that to happen.

Fretted surfaces usually have high roughness, which may induce cracks and function as initiation sites for fatigue cracks. No solution has been found to prevent fretting, but reducing the coefficient of friction or the slip amplitude can result in less damage caused by this wear mode. Another possible solution for reducing damage in some cases might be to roughen the surface even more, which would then create escape routes for the debris generated in the interface, avoiding them to become even more harmful as a third body [5][45].

Zhu [6] published a thorough review of fretting wear modes, which is summarized in the following.

There are four modes under which fretting wear might occur in a sphere-to-flat configuration: tangential, radial, rotational and torsional fretting, as seen in Fig. 2.9.

Tangential fretting is the most common mode studied, due to the availability of testers and high number of similar studies reported in the literature, being also called classical fretting. With increasing sliding amplitude, the wear regime changes from partial-slip (PS), where the central zone of the contact area is governed by adhesion and micro-slip occurs in the outer region, to gross-slip (GS), where one surface slips completely on the other inside the contact

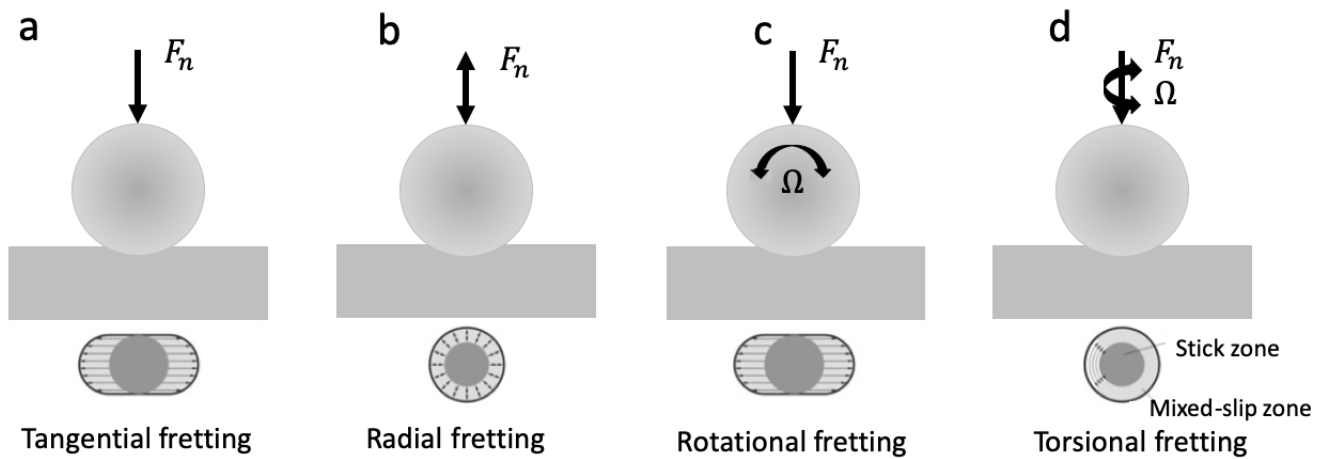


Figure 2.9: Four simple fretting modes for sphere-to-flat configuration: a) Tangential Fretting, b) Radial Fretting, c) Rotational Fretting, d) Torsional Fretting. Reproduced from [6].

area.

Radial fretting is mainly induced by varying normal loads, and no impact occurs, since the two surfaces remain in contact. A typical wear scar generated by radial fretting is shown in Fig. 2.10.

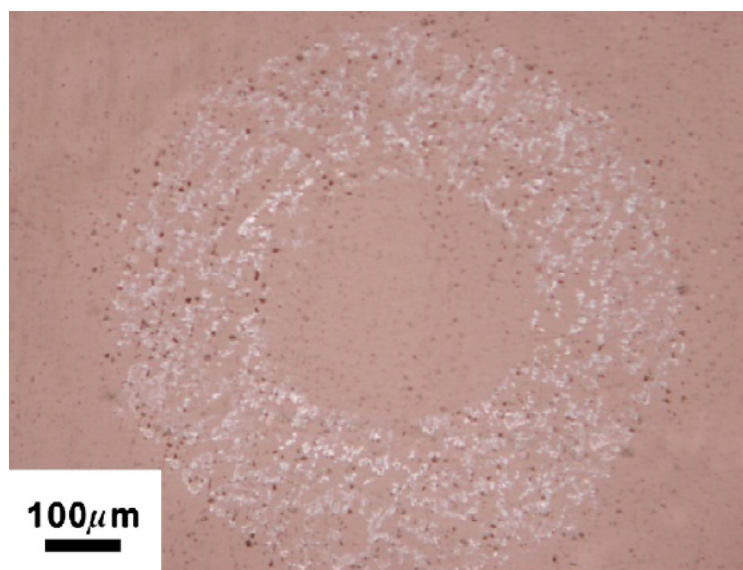


Figure 2.10: Typical optical morphology of radial fretting scar for a dental ceramics. Extracted from [6].

Rotational fretting produces wear marks in a similar manner to those due to tangential fretting. This wear mode consists in the oscillatory rolling of a spherical sample over a flat counterpart, in such a way that there is always a region of the sphere which is intermittently in contact and out of contact with the flat surface. The evolution of wear scars for a rotational fretting wear test is showed in Fig. 2.11.

Torsional fretting is the wear mode studied in this work. Zhu [6] observed that with the increase of the angular displacement amplitude, the extents of the detachment and plastic

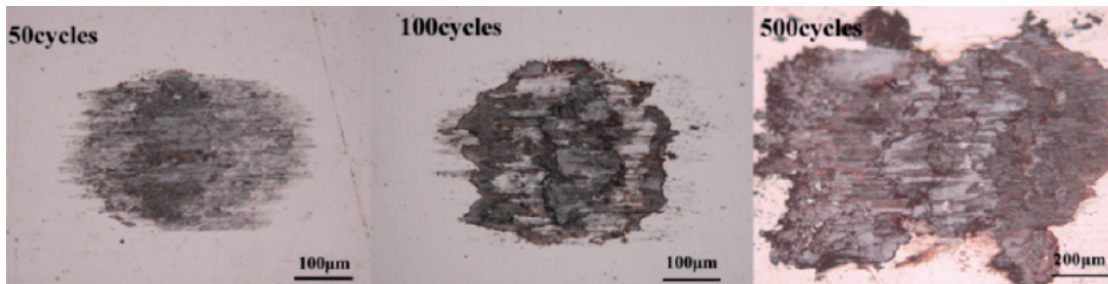


Figure 2.11: Evolution of wear scars of rotational fretting for LZ50 steel, normal load of 10 N and angular range of $\pm 0.25^\circ$. Extracted from [6].

flow of material develop gradually, along with an increase of tribo-oxidation. He also pointed out, as discussed previously, that the tribo-oxidation in this wear mode is strongly dependent on the humidity of the environment. For this mode, the wear regime changes from a partial-slip regime for low angular ranges, to a mixed-regime at intermediate values of angular displacement, where a clear annular outer area is seen in contrast with a central adhesion zone, and finally to a slip-regime for high angular oscillation, where the whole mark shows severe wear damage. It should be noted that, as seen in Sec. 4.2, the cases studied in this work fall in the mixed-regime.

As for the wear mechanisms that take place in torsional fretting, it is worth noting that in mixed regime, they can be summarized in abrasive wear, oxidative wear and delamination. However, in the slip-regime, i.e., for high values of angular range and number of cycles, thicker debris layers rest on the scar, but the wear mechanisms are also a combination of the aforementioned phenomena. The morphology a scar created by torsional fretting wear for 7075 steel alloy is shown in Fig. 2.12 [6].

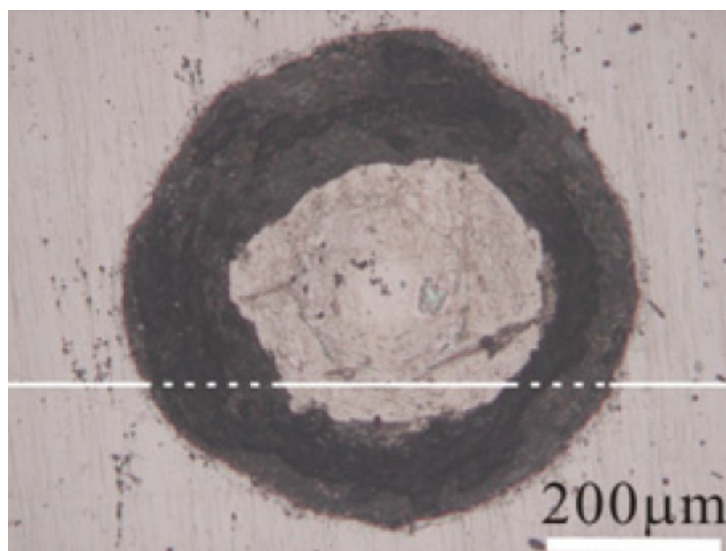


Figure 2.12: Scar morphology of torsional fretting wear for 7075 steel alloy, with normal load of 100 N, angular displacement of $\pm 0.5^\circ$ and 5,000 cycles. Extracted from [6].

2.3 Microscopy analysis and wear volume estimations

In traditional fretting wear tests, namely, tangential fretting, testers are widely available and may even provide wear volume and wear rate estimations. When those values are not promptly output by the machine, the wear marks are relatively easy to inspect. Confocal and scanning electron microscopes are usually chosen to analyze those wear scars, since they are able to provide accurate measurements of the parameters needed to calculate wear volume and, consequently, wear rates. Those calculations may be carried out manually by the user, by means of Eq. (2.9), for example, or more specific empirical equations developed for a certain contact configuration.

Since the scar's profile is basically composed of peaks and valleys of deposited and removed material, one way to estimate the worn volume of a surface is by calculating the "positive" volume above the original surface level and "negative" volume below it. Those values, when calculated for both surfaces and summed up should result in the total worn volume, disregarding the amount of material completely ejected from the contact interface. This method is shown in the literature (see [52]).

Profilometric studies for different combinations of metals showed three basic types of fretting wear situations in the sphere-to-flat configuration, regarding the deposition and removal of material from the surfaces in contact. The first case is when there is very little metal transfer between the materials and wear is even for both of them. The second case is when, due to sphere's material being much harder than the flat surface, a heavy transfer of metal occurs from the flat sample to the spherical one, and deep grooves are found in the softer material. The last case is when a heavy build-up of material on the flat surface occurs. This accumulation is attributed to a back transfer of material originally removed from the flat sample and adhered to the sphere, and also to plastic flow of the flat surface [52].

Torsional fretting wear tests, however, have not been conducted extensively enough for methods for calculating wear rates to be firmly established by the literature. However, a few approaches to that problem are described in the following.

For torsional fretting wear, since there is no sliding length clearly defined, it is not viable to use Archard's equation for estimating the wear rate. Adapting his formula by replacing the sliding distance with a circumference's arc is not feasible, since the radius of the circumference itself changes with time, as the contact area increases. It is possible, however, to define wear rate the ratio of worn volume to the number of wear cycles. Thus, one must only determine the volume of displaced material from each surface and the wear rate would be attained. Nevertheless, estimating the wear volume is not always a straight forward task.

Considering the sphere-to-flat configuration, it is possible to generate very regular, circular wear marks. That happens mostly when the sphere is much harder than the flat sample and the latter is made of a very soft material, such as elastomers or polymers, in general. In that case, one might measure the volume of the wear crater by analyzing a two-dimensional

profile of the mark. By measuring the scars' diameter, d , and depth, h , one could calculate the worn volume, V , through the very definition of a spherical cap geometry. Namely,

$$V = \frac{1}{6}\pi h \left(\left(\frac{d}{2} \right)^2 + h^2 \right) \quad (2.17)$$

It should be noted that similar methods have been reported in the literature for micro-scale abrasion and wear tests [53, 54].

However, when wear damage is considerably done on both surfaces, which is the case for most metal against metal contacts, the scars usually do not show a regular shape. They might have irregular edges, lots of peaks and valleys and distinct zones with very different depths, such as central adhesion zone and an outer annular mixed-slip region, as discussed before. In those situations, the estimation of the worn volume might rely on computational tools that are able to perform a similar calculation as that described above, where a reference line is established, and the volumes above and below it are computed. A more in-depth discussion of such a method for the specific case of this work is shown in Sec. 3.4.4.

Chapter 3

Materials and Methods

This work aims to study the contact between R3 offshore steel and PC/ABS under torsional fretting wear. More specifically, to analyze the worn surfaces of both materials, measure the worn volume and determine whether this specific polymer blend is suitable for coating the steel chains found in mooring systems, so as to reduce the damage caused by the contact. In order to do so, an experimental setup was developed and a test matrix was designed.

3.1 Experimental Setup

The experimental setup consisted of specially machined tools made of R3-graded offshore steel, with a cylindrical body and a hemispherical tip with a 7.5 mm radius. Prismatic counterparts (from here on also called pads) made of R3 steel and PC/ABS 60:40 were used, all with 20mm x 20mm x 5mm dimensions. The contact pair can be seen in Fig. 3.1

The R3 samples were manufactured by a CNC machine with tolerance of $\pm 0.1mm$ and consisted of material directly removed from standard 120D mooring chain links. The PC/ABS samples, made by injection molding, were supplied by SABIC.

In order to firmly accommodate the prismatic pads, a custom holding device was used (see [7]), as can be seen in Fig. 3.2.

A MTS 809 axial-torsional testing machine was used. It has a 25 kN actuator and can perform tests with axial and rotational motion simultaneously, which is ideal for the tests conducted in this research. The experimental setup, with both the hemispherical tool and the counterpart inside the holding device, both inserted in the testing machine, is depicted in Fig. 3.3

The surface analysis of the worn parts was conducted on a confocal laser microscope (Olympus LEXT OLS4100, see Fig. 3.4) and on an optical microscope (Carl Zeiss AXIO Imager M2, see Fig. 3.5). A thorough explanation of the experimental procedure is shown



(a) R3 steel pad and R3 steel flat counterpart.



(b) R3 steel pad and PC/ABS 60:40 flat counterpart.

Figure 3.1: Depiction of representative specimens of each test configuration.

Table 3.1: Mechanical properties of the R3 offshore grade steel and the PC/ABS 60:40 blend.

Material	R3 offshore steel	PC/ABS 60:40
Young modulus, E (GPa)	207	2.2
Poisson's coefficient, ν	0.34	0.35
Yield stress, σ_y (MPa)	410	54

in Sec .3.4.

3.2 Materials

This section aims to describe the materials used in more detail.

The steel used was a R3-graded offshore naval steel, extracted directly from an actual mooring chain link, supplied by CENPES/Petrobras. This offshore grading is sometimes broad in its classification parameters, but for a steel to be classified as R3, it must show minimal values of certain properties, all of which are standardized [17].

The polymer blend used is a Polycarbonate/Acrylonitrile-Butadiene-Styrene (PC/ABS) with a 60:40 weight ratio of PC to ABS. This blend, as explained in Sec. 1.1 is a strong yet soft material, ideal for being applied as coating for the mooring chains. The specific blend used in this work was produced by SABIC, by injection molding. Most properties for both materials were provided by their manufacturers and technical standards, with exception of the Poisson's ratio for the PC/ABS, which was retrieved from [55]. The relevant properties of both materials are show in Tab. 3.1

Prior to the wear tests (which are described in 3.3 and 3.4), micro-hardness experiments



Figure 3.2: Holding device (version 1.1 [7]) used for the flat specimens.

were conducted using a Vickers micro-indenter (HM2000 Fischer Technology) with a 0.1 N load. This method is able to capture hardness variations on the most superficial layer, indicating whether the material has a homogeneous surface. Moreover, a universal hardness tester (ZHU 250) was used to evaluate the materials' standard hardness, using a Brinell test with a 2.5 mm tungsten carbide sphere and a load of 300 N (HBW 2.5/300). This specific indenter was chosen for two main reasons, namely: i) its shape resembles the hemispherical pad used in the wear tests, and ii) it has a wide scale for evaluation of the mean combined hardness of surface and substrate. For each material, 3 measurements were taken on three different flat samples. The results are seen in Tab. 4.1.

3.3 Test Program

In order to attain consistent and relevant results, a test program was designed. The wear tests consisted in establishing contact between the hemispherical tip of the tool and the flat surface of the counterpart, applying a determined normal load on the surface and, while keeping that pressure constant, rotating the tool with a predetermined angle range for a certain number of cycles, at a fixed frequency.

The reference condition for this research was R3 against R3, to emulate the current condition under which the chain links contact one another on the field. That way, the difference of using PC/ABS instead of R3 as a counterpart would be clearly noted. Therefore, tests were made with both R3 x R3 and R3 x PC/ABS 60:40. An overview of the wear tests program can be seen in Tab. 3.2. It should be noted that every test on Tab. 3.2 was done for R3

Table 3.2: Wear tests program matrix

Load	# of cycles	Frequency [Hz]	Angle range	# of tests
1.0 kN	0	0	0	2
1.0 kN	50,000	5.0	$\pm 1.0^\circ$	2
1.0 kN	100,000	5.0	$\pm 1.0^\circ$	2
1.0 kN	200,000	5.0	$\pm 1.0^\circ$	2
2.0 kN	0	0	0	2
2.0 kN	50,000	5.0	$\pm 1.0^\circ$	2
2.0 kN	100,000	5.0	$\pm 1.0^\circ$	2
2.0 kN	200,000	5.0	$\pm 1.0^\circ$	2

x R3 and R3 x PC/ABS. The load values were obtained in previous studies [32] and were chosen in order to promote mild and severe elasto-plastic strains. Therefore, 32 wear tests were conducted in total.

3.4 Experimental Procedures

The experimental procedure can be summarized in four main steps: 1) Preparation of the samples; 2) Pure compression phase; 3) Torsional fretting wear test; 4) Microscopy analysis.

Each step is detailed in the following.

3.4.1 Preparation of the samples

Prior to every torsional wear test, the samples were carefully prepared. First, the flat counterpart was ground in a rotational wet sanding machine with a gradual refinement of the sandpaper, i.e., 120, 240, 400, 600, 800 and 1200 grid. Hence, it was assured that the samples' surfaces were ground to similar roughness levels and no abrupt grinding defect was generated. All samples were controlled for a minimal roughness of $Ra_{min} = 0.4$ and a maximum dimensional distortion of 1° .

All samples and hemispherical tools were carefully cleaned with isopropyl alcohol and stored in individual zip lock bags. Immediately before the wear tests, a pair of sample and tool was removed from the storage bags, carefully examined for any visible contaminants or imperfections, and only then mounted on the testing machine. This reduced the chance of considerable oxidation occurring before the test itself.

After the tests were complete, dust or loose particles/contaminants were removed from the surfaces of both tool and flat sample by a compressed air gun, which were then stored in new, separate zip lock bags.

3.4.2 Pure compression phase

Fig. 3.6 depicts the contact configuration employed in this work, and highlights the displacement and rotation restraints imposed (see Fig. 3.6a), as well as the loading condition (see Fig. 3.6b). Namely, the hemispherical pad's lateral face (marked in red) is fully restrained while the flat sample's side faces and bottom have normal displacement restraints. A more detailed explanation is given, as follows.

Once the samples were prepared, the wear tests were conducted. As said before, these tests were done on a MTS axial-torsional testing machine. This system consisted of two actuators, inside which one might insert different types of specimens, depending on the collet used. An appropriate collet for housing and clamping the holding device shown in Fig. 3.2 was used in the lower actuator, which could be controlled both manually and remotely. The upper actuator, which held the hemispherical tool, could only be manually displaced.

It should be noted that, because of the many variables involved in setting up these tests, a procedural algorithm was developed to precisely reproduce the experiments here described, which can be found in Appendix I. Nevertheless, a thorough explanation of the experimental procedures is given as follows.

First of all, as said before, a pair of tool/pad appropriately prepared was selected, following the test matrix, and assembled in the testing machine, i.e., the hemispherical tool was placed inside the upper grip and the counterpart (after inserted in the holding device), was gripped by the lower actuator. At this point, there was a significant distance between the materials.

Using the Basic Testware software provided with the testing machine, the test parameters were selected so as to perform the first part of the mechanical test, namely, applying the normal load on the sample. In order to do that, the desired load was set on the software and, after manually displacing the upper grip towards the lower one, the software would slowly rise the flat pad in the direction of the tool. This was performed at a fixed speed of 0.5 mm/min. The program was set to stop moving the pad when it reached the desired load. After that, the pair remained fixed in place, with the contact pressure constant and equal to the preset value.

3.4.3 Torsional fretting wear tests

Following that, another software provided along with the machine by the manufacturer, i.e., MPE TestSuite, was used to execute the second part of the test, namely the actual torsional fretting wear motion. In this program, a block diagram was made in such a way that would assure the normal load to remain constant (by moving the flat sample up or down, as needed), while performing the rotational motion. The angle range was set up to $\pm 1.0^\circ$ and the rotational frequency to 5 Hz for all the tests. For each run, the number of cycles and

the normal load were selected, and the test was constantly monitored by plots of the instantaneous normal load. Upon reaching the total number of wear cycles, the machine would stop.

Both sample and tool were carefully removed from the machine, visually inspected for any abnormalities, and promptly cleaned with a compressed air gun. This removed debris accumulation and other loose particles on the surfaces of the materials. The pair was then placed in separate bags, cataloged and stored for future microscopy analysis.

3.4.4 Microscopy analysis

After removing and storing the tested samples, they were analyzed in a confocal laser microscope, as previously explained.

First, the flat samples were placed on the microscope's table, and the software was initialized. All samples were analyzed with a 20x magnification lens, which were focused manually for each specimen. A stitching procedure was done to capture all the wear mark, in both laser and color spectrum with $1.0 \mu m$ steps. Because PC/ABS 60:40 has a darker surface, approximately 60% level brightness was used to fully encompass the details on its surface. However, considering the reflective nature of steel, lower brightness levels were used to analyze the R3 samples, namely, around 40% for the color spectrum and 20% for laser.

Then, after the image was stitched, a few analysis were made. The objective was basically to evaluate the volume of removed material due to wear. Two approaches were taken to accomplish that goal.

The first method employed was to measure the volume of the wear crater by analyzing a two-dimensional profile of the mark, as described in Sec. 2.3. Values for the diameter in XY and XZ planes were taken and compared, so as to evaluate the eccentricity of the scars and determine an average value, used in Eq. (2.17).

It is evident that Eq. (2.17) is suitable only when assuming the wear mark to be spherical. This method worked very well for R3 x PC/ABS, since the wear marks had very low eccentricity. For this method to work, a reference line was placed on the surface level of the sample, and another one on the lowest point of the cross-sectional profile. The first reference line also had its extreme points set to the edges of the wear mark, so that the diameter of the scar would be measured.

However, for R3 X R3, this method was not appropriate, since the scars had irregular shapes and could not be approximated, with any considerable accuracy, to spherical caps (see Fig. 3.8b). This discussion is explored in more detail, along with the results of such measurements, in Sec. 4.3.

The second approach, applied for R3 samples, consisted in using a computer-aided vol-

ume measurement tool, embedded in the microscope's software, as mentioned in Sec. 2.3. This required manual definitions of a reference line for the surface and a zone of interest. After defining those parameters, the software would calculate the volume below or above the reference surface, but only inside the zone of interest.

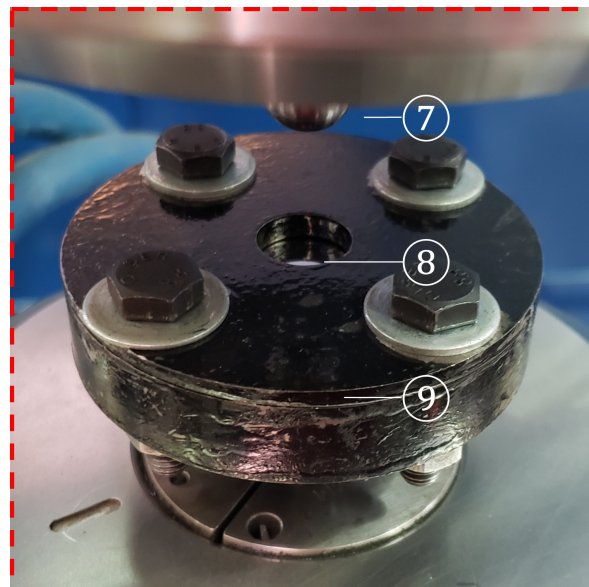
Representative images of both methods are shown in Fig. 3.7 and Fig. 3.8.

Finally, the hemispherical tools were also analyzed. For the R3 x PC/ABS configuration, no signs of damage to the tool were seen. However, for R3 x R3, significant deformation and wear were noted on some tools' tips. Because of that, those tools were also inspected on the confocal laser microscope, as well as on an optical one. Since they were made of R3 steel, all tools were inspected similarly to the R3 flat samples, including the volume measurement method chosen.

On the optical microscope, various settings were used, and the goal was simply to determine if considerable damage was done to the tip, before bringing it to the confocal laser microscope.



(a)



(b)

Figure 3.3: Experimental setup for the wear tests. Machine used: MTS 809 Axial-Torsional. (a) Equipment: 1) Crosshead, 2) Force transducer, 3) Top cell, 4) Upper grip, 5) Lower grip, 6) Bottom cell. (b) Detailed view of the specimens: 7) Hemispherical pad, 8) Flat sample, 9) Holding device.

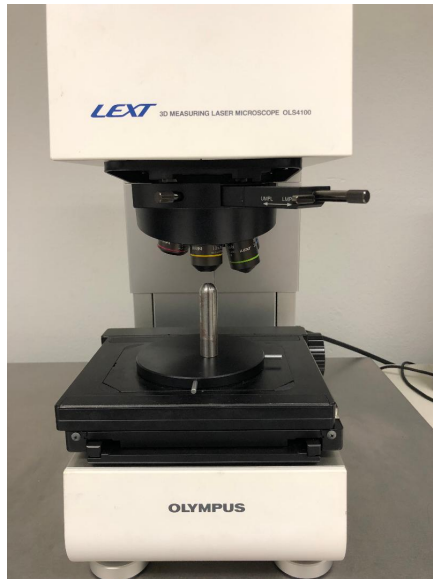


Figure 3.4: Olympus LEXT OLS4100 confocal laser microscope.



Figure 3.5: Carl Zeiss AXIO Imager M2 optical microscope. Extracted from manufacturer's catalog.

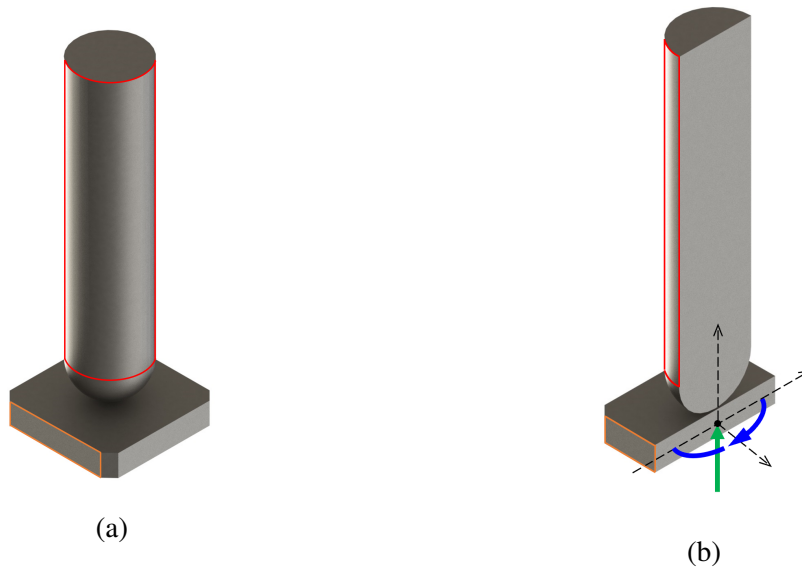


Figure 3.6: Illustration of the contact configuration, restraints and loading conditions used. (a) Encastre on the hemispherical pad (red area) and lateral face constraint (orange area); (b) normal load and z-axis rotation.

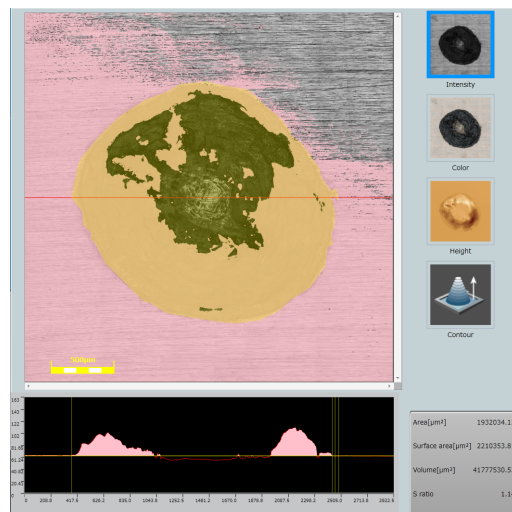


Figure 3.7: Computer-aided volume measurement method. Applied only to R3 samples.

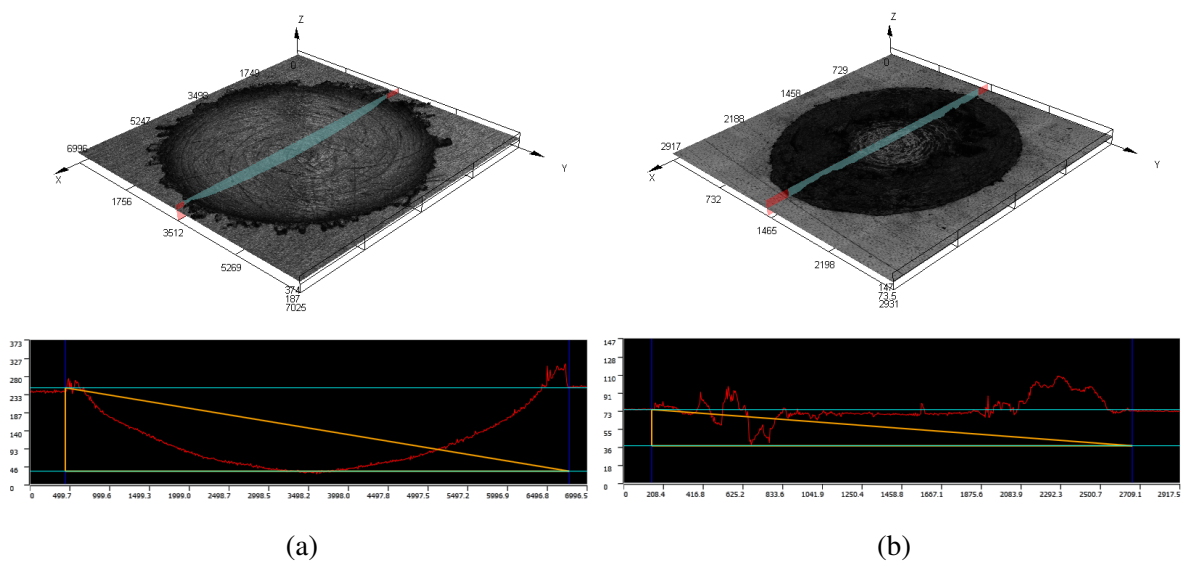


Figure 3.8: Representative 3D (top) and 2D (bottom) profiles of flat samples used for quantifying the wear volume, by measuring the scar's depth and diameter. (a) PC/ABS 60:40 ; (b) R3 steel.

Chapter 4

Results and Discussions

This research, as outlined before, focused on evaluating the wear effects of a torsional fretting motion between R3 steel tools and PC/ABS 60:40 samples, and on comparing those to pairs of R3 specimens, tested the same way. The main goal of this work was to determine whether this specific polymer blend would be a suitable candidate for coating R3 mooring chain links, so as to extend their lifetimes.

Based on the methodology explained in Chapter 3, measurements regarding hardness, contact zones' depth, diameter and volume were made. The results presented in this chapter shall be divided in four parts, namely: 1. Hardness of the materials; 2. Scar morphology; 3. Wear analysis; and 4. Life estimations.

4.1 Hardness of the materials

As explained in Sec. 3.2, hardness tests were performed on flat samples of both materials prior to the wear tests. The results are shown in Tab. 4.1.

Examining Tab. 4.1, it can be observed that, as expected, the values for R3 offshore steel are much higher than those for PC/ABS 60:40, namely, R3 steel is $\approx 77\%$ harder than this polymer blend. One expects that, when pairing materials with such a significant difference

Table 4.1: Hardness of the flat counterparts.

	R3 steel	PC/ABS 60:40
HV0.1	198±5	122±14
	199±2	120±8
	198±4	115±3
HBW 25/300	183±7	103±2
	188±12	105±3
	186±2	104±2

in hardness, most (if not all) appreciable damage would be made on the softer surface. That is indeed the case, as shown in Sec. 4.2.

Still regarding the hardness measurements, two important observations must be made. First, the difference in micro-hardness and standard hardness values is small (the maximum difference observed in nominal images is around 8% for R3 steel and around 18% for PC/ABS 60:40), which indicates that the materials were homogeneous in depth. Secondly, the maximum standard deviation observed in the repeated tests for a determined material was around 11%, meaning that, throughout the surfaces, hardness was also considerably constant. Given these two observations, the particles removed by wear should have fairly constant hardness.

4.2 Scar Morphology

The stitched images obtained from the confocal laser microscope provide a high level of detail and revealed interesting aspects regarding the morphology of the worn surfaces. Immediately after cleaning the tested samples, i.e., only by visual inspection, some observations were made.

First, for all compression tests, i.e. with 0 cycle of torsional fretting, the tools' tips were intact, indicating no damage was done on them. Moreover, smooth and regular circular marks were attained on the flat samples, which were barely visible, given the low indentation depth. Because of that, those results will be discussed in Sec. 4.3.

Secondly, in the tests involving R3 x PC/ABS 60:40, the hemispherical tools were also intact, even at the most critical condition, i.e., 2.0 kN and 200,000 cycles. That is probably because of the great difference between the materials, mainly with respect to their hardness, as explained in Sec. 4.1.

However, for the R3 x R3 pairs, appreciable damage was generated for every condition involving wear cycles, but not for pure compression.

Top-view images representing each test configuration for the reference condition and for R3 x PC/ABS 60:40 are shown, respectively, in Fig. 4.1 and Fig. 4.2. Since damage was done to the tools only in the reference condition, images of their tips are shown only for this configuration. It should be noted that, due to changes in shape and overall dimensions of the wear scars, the scales used were not kept constant.

Analyzing Fig. 4.1, one can promptly identify two distinct regions on every image, namely, an adhesion zone (mostly in the center of the contact area) and an annular partial-slip zone, surrounding the first, as expected.

It is interesting to note that, because of the strong adhesion occurring in the central zone, almost no indentation nor severe damage is observed, indicating that the surfaces in this region were, indeed, stuck to each other, or at least, barely moving. The result is a smoother

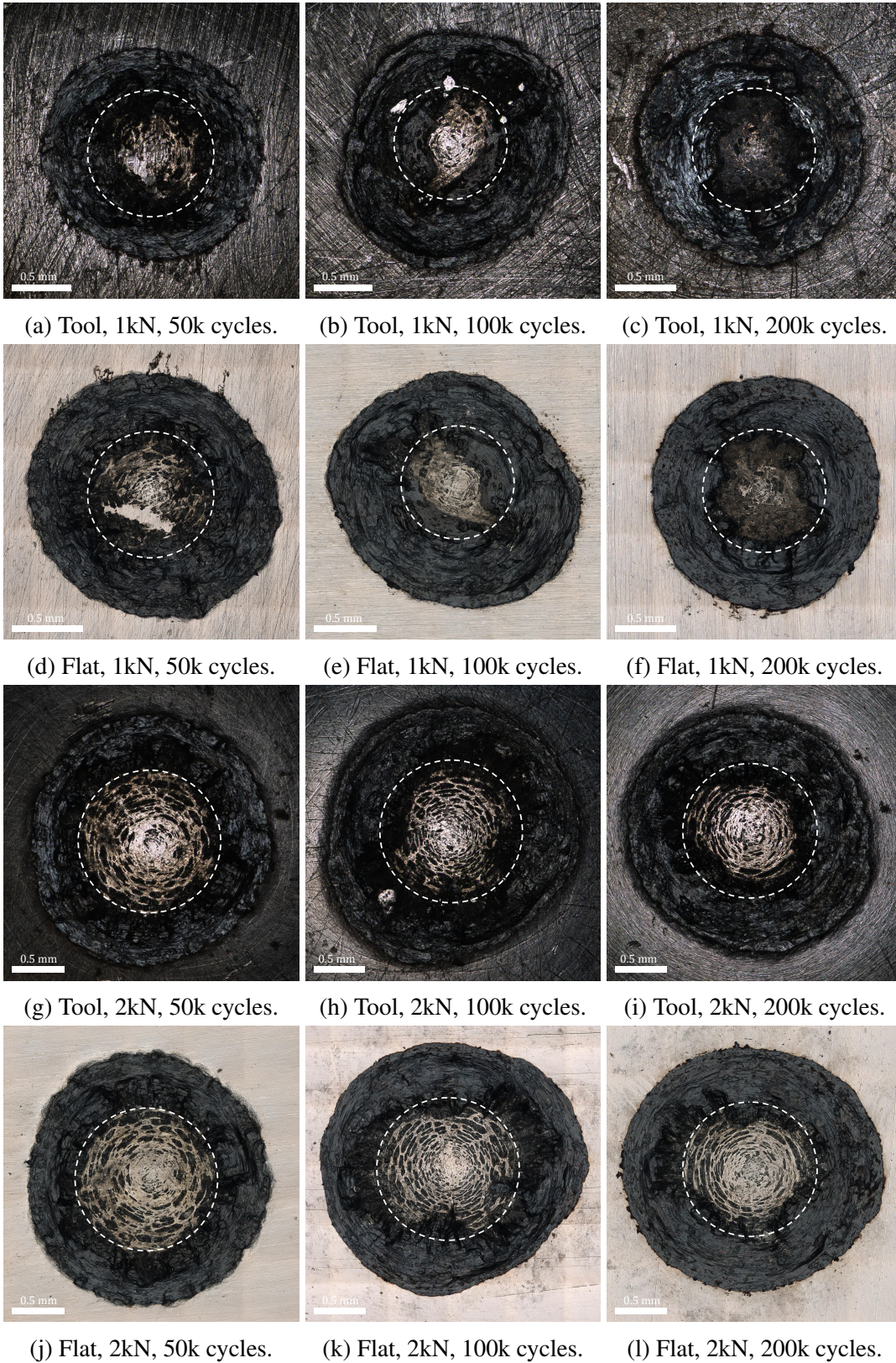


Figure 4.1: Two dimensional profiles of the R3 steel flat counterparts and hemispherical tools' tips.

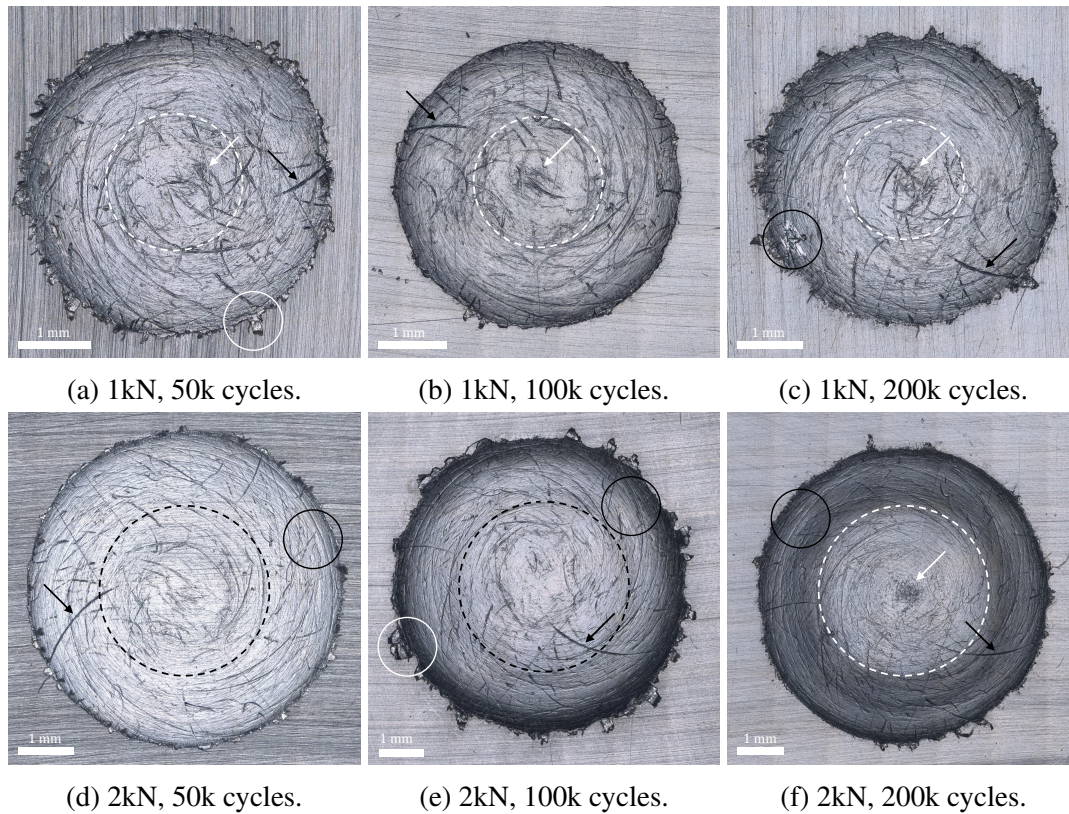


Figure 4.2: Two dimensional profiles of the PC/ABS 60:40 flat counterparts.

zone, with an appearance similar to that of the original surface. However, in the partial-slip region, severe wear damage is found, characterized by a very rough area, with irregular shape and filled with grooves and peaks of material.

Those preserved inner adhesion zones, found in the reference condition and shown in Figs. 4.1d-4.1f and 4.1j-4.1l have also been found by others in similar researches. Wang [56], for instance, performed experiments on torsional fretting wear of 1045 steel against a monomer cast nylon filled with glass fiber. He found scars with the same characteristics as the ones here described, namely, a central region with negligible indentation and an annular zone with severe wear damage.

It is also important to note that, in all tests with R3 x R3, a curious pattern is seen in the central zone, and can be found in both tool and flat counterpart surfaces. This pattern is apparently produced by a chipping effect, and becomes more evident for 2.0 kN loads, when the adhesion zone is around 18% to 22% larger than for 1.0 kN. An explanation for this effect is proposed as follows. Wear debris generated during the torsional fretting motion may have various effects on the surfaces. The smallest debris produced in the mixed-slip zone might be brought to the central area due to the relative angular motion of the surfaces, and crushed into even smaller particles. They could, then, be stuck at a fixed point on the interface and gradually chip off material from both sides during each cycle.

Three observations should be made about this pattern effect, namely:

1. The chipping marks became more slender as the number of cycles increased;
2. The depth of those marks seems to be independent, or at least not highly altered by the number of cycles;
3. The marks get larger as one moves away from the first point of contact.

The first two trends above described can be seen in Fig. 4.1. The third observation is depicted in Fig. 4.3, obtained from the optical microscope, which shows the tip of the tool used in a test with 1.0 kN and 200,000 wear cycles. In that image, one can promptly see that the marks get larger in regions more distant from the first point of contact. It also shows that the marks are actually small in absolute size, the bigger ones, in this specific condition, having around 100 μm in length, but relatively large when compared to the adhesion zone. These observations indicate that, indeed, the debris get smaller as the number of wear cycles increases.

It should be noted that, even though dark red powder was found on the surfaces for some conditions immediately after the tests (as expected and explained in Sec.2.2.5), no oxidation was observed on the samples during the microscopy analysis. Therefore, one can conclude that any particles that were eventually present in the wear marks after the tests were completely removed by the cleaning procedure with compressed air.



Figure 4.3: Detailed view of the chipping patterns on the tip of a hemispherical tool. Test conditions: R3 x R3, 1.0 kN, 200,000 cycles.

Regarding the annular, partial-slip zone, severe damage was found. Namely, the marks show grooves, peaks and lumps irregularly spread through the surface, indicating exchange of material between tool and counterpart. In most cases, the overall shape of the scars was circular. However, marks with higher eccentricity, i.e. more elliptical, were also seen, e.g. Figs. 4.1b and 4.1e.

A very different scenario was seen for the PC/ABS 60:40 samples. As said before, the tools in these cases remained intact, so that all deformation and wear damage found on the polymer samples was done on the flat counterpart. Overall, the scars shown in Fig. 4.2 have smooth, hemispherical shapes, with no abrupt transition from the adhesion zone to the mixed-slip region.

The damage seen on these marks are mostly scattered scratches, likely generated by wear debris, although a few deeper dragging scars can be found, as pointed out by the black

arrows, which are indication that some particles may have been stuck in place during a number of cycles. However, since most of the scratches are shallow (much differently from the chipping marks found on R3 x R3 configuration), it can be inferred that most debris created during the tests were rapidly pushed away from the contact area. Another important feature to note is that micro-fractures and cracks were found on the edges of the contact marks, indicated by white arrows in the images.

Still regarding Fig. 4.2, one can see that, with increasing load, the samples show increasingly smoother surfaces. Indeed, the comparison between Fig. 4.2b and Fig. 4.2e, for instance, reveals that, for the same number of cycles, a sample tested under 2.0 kN shows considerably less scratches, but deeper wear grooves on the edges. A possible explanation for that is as follows. Being a much softer material, not as nearly affected by oxidation as R3 steel, the PC/ABS debris formed during the tests managed to escape the contact zone more easily when the normal load was lower, namely, 1.0 kN. Doubling the load to 2.0 kN may have resulted in those same debris being smashed again onto the surface or even not generated at all, given the intense deformation promoted by this load.

A final note must be made to the apparent polishing effect created at the edges of some contact zones, indicated by black circles on the images. Once again, these observations point to a decrease of the number of debris with increasing load and number of cycles, similarly to what was seen for R3 x R3.

4.3 Wear Analysis

As explained in Sec. 3.4.4, different approaches were taken to evaluate the wear volume of the tests. For the reference condition, a computer-aided volume measurement tool was used, since the marks were sometimes highly eccentric and could not be approximated by a spherical cap. It was mentioned in Sec. 4.2 that material was exchanged between tool and counterpart. Therefore, it was practically impossible to determine what fraction of the displaced volume came from one or the other. Furthermore, there was no regularity in the material exchange. Indeed, in some cases, it was evident that almost all the displaced volume was actually due to deposited material on the other side of the interface. A case like this can be seen in Fig. 4.4, which shows a three-dimensional profile of the surfaces of a contact pair for the reference condition.

Most cases, however, showed a highly non-linear, complex exchange of material. The best way found to evaluate the displaced volume was the following. For a given pair, each side of the interface was analyzed separately. Measurements using the software tool were made using a reference line for the original surface level, and a custom-drawn zone of interest, as shown in Fig. 3.7. By doing so, the volume above or below the reference level and simultaneously inside the region of interest was calculated. Results for these measurements are show in Tab. 4.2, where V^+ , V^- and V_w represent, respectively, the volume of mate-

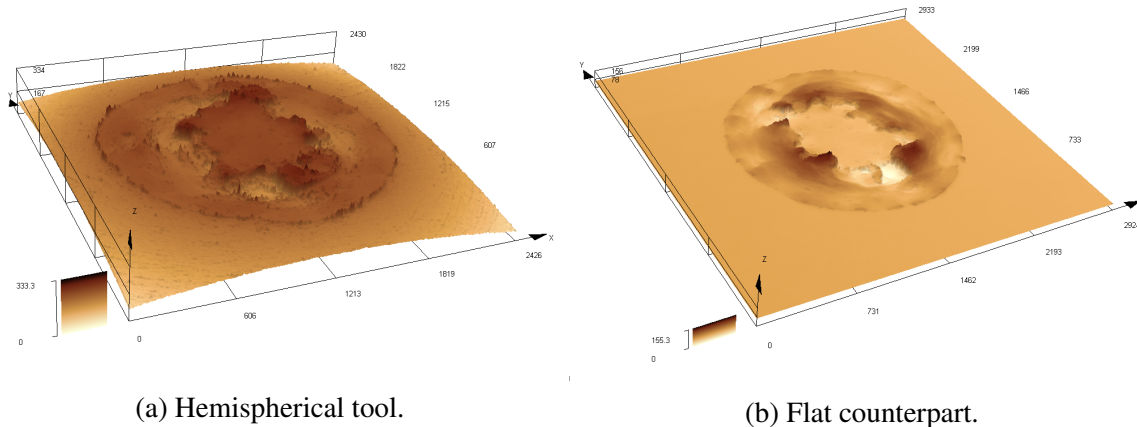


Figure 4.4: Three dimensional profiles of the R3 steel samples. Test conditions: 1.0 kN, 200,000 cycles.

rial above the reference line, the void below the reference line and the net worn volume of the interface. It is worth noting that, for pure compression tests, the volume was calculated the same way as for the PC/ABS samples, i.e., by approximating the scar's geometry to a spherical cap.

A more careful analysis showed that, even though wear occurred at 50,000 cycles, no considerable volume of material was actually lost. Rather, the displaced matter from the flat samples could be found deposited on itself (at the outer regions of the scars) and on the central zone of the hemispherical tool. At higher number of cycles, namely, 100,000 and 200,000, considerable material exchange was found. As said before, it is not straightforward to determine where each unit volume came from.

The evolution of wear volume for R3 x R3 configuration, with respect to the number of cycles is shown in Fig. 4.5 for both load levels.

A few observations can be made from the analysis of the results presented in Fig. 4.5. Namely,

- Comparing the marks' volumes for pure compression, i.e., 0 cycle, it is clear that, increasing the load by 2 times results in a 6-fold increase in displaced volume, showing the high influence of the normal load in the contact zone during compressive deformation. Moreover, the running-in phase is inferred to happen and probably lasted less than 50k cycles. This non-linear initial stage of the tests will be disregarded, so that a coherent and more reliable analysis after the stabilization of the wear phenomena can be made, as done by [57].
- Defining the wear rate as the ratio between net wear volume and number of cycles, it is observed that for the 2.0 kN tests, the wear rate ($\approx 0.17\mu\text{m}^3/\text{kilocycle}$) is around two times higher than for 1.0 kN tests (which is $\approx 0.08\mu\text{m}^3/\text{kilocycle}$);

As explained before, the analysis for PC/ABS 60:40 was much simpler. Namely, because

Table 4.2: Volume measurements: reference configuration.

Condition	Flat		Pad		Interface
	$V^+[\text{mm}^3]$	$V^-[\text{mm}^3]$	$V^+[\text{mm}^3]$	$V^-[\text{mm}^3]$	$V_w[\text{mm}^3]$
1kN, 0 cycles	-	-	-	-	0.003 (†)
	-	-	-	-	0.003 (†)
1kN, 50k cycles	0.020	-0.012	0.020	0.000	0.028
	0.025	-0.019	0.026	0.000	0.032
1kN, 100k cycles	0.031	-0.012	0.018	0.000	0.037
	0.042	-0.011	0.036	-0.028	0.039
1kN, 200k cycles	0.035	-0.008	0.029	-0.014	0.042
	0.030	-0.007	0.025	-0.005	0.043
2kN, 0 cycles	-	-	-	-	0.018 (‡)
	-	-	-	-	0.018 (‡)
2kN, 50k cycles	0.036	-0.046	0.071	0.000	0.061
	0.023	-0.013	0.049	0.000	0.059
2kN, 100k cycles	0.047	-0.013	0.082	-0.040	0.076
	0.061	-0.012	0.055	-0.037	0.067
2kN, 200k cycles	0.077	-0.017	0.032	-0.002	0.090
	0.062	-0.034	0.066	-0.011	0.083

† Spherical indentation volume for the 1.0 kN load.

‡ Spherical indentation volume for the 2.0 kN load.

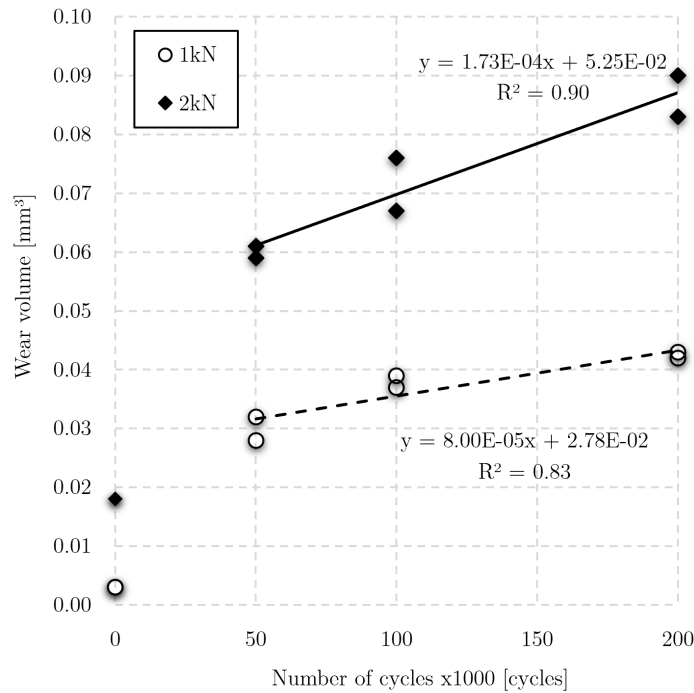


Figure 4.5: Net wear volume versus number of cycles: reference configuration (R3 x R3).

Table 4.3: Volume estimations: PC/ABS 60:40 flat counterpart.

Condition	d_x [mm]	d_y [mm]	h_x [mm]	h_y [mm]	V [mm ³]
1kN, 0 cycles	2.879	3.102	0.013	0.011	0.042
	3.186	3.207	0.013	0.016	0.059
1kN, 50k cycles	3.869	3.978	0.053	0.048	0.307
	4.053	3.996	0.055	0.050	0.333
1kN, 100k cycles	4.159	4.107	0.059	0.053	0.379
	4.058	4.039	0.056	0.051	0.347
1kN, 200k cycles	4.229	4.271	0.073	0.076	0.529
	4.307	4.299	0.084	0.085	0.615
2kN, 0 cycles	4.480	4.271	0.052	0.054	0.404
	4.192	4.335	0.031	0.033	0.229
2kN, 50k cycles	5.579	5.625	0.149	0.142	1.799
	5.773	5.809	0.203	0.202	2.670
2kN, 100k cycles	6.252	6.297	0.261	0.252	3.970
	6.194	6.244	0.222	0.221	3.370
2kN, 200k cycles	6.785	6.874	0.345	0.361	6.485
	6.149	6.242	0.309	0.322	4.773

there was no material transfer from the tool to the flat samples, and the marks had very low eccentricity, the best approach to evaluate the scars' volumes was to calculate a spherical cap volume correspondent to the depth and diameter of the measured mark. The results are shown in Tab. 4.3, where d_x , d_y , h_x and h_y represent, respectively, the diameters and depths measured in both horizontal and vertical directions (see Fig. 3.8) and V corresponds to the volume calculated by Eq. (2.17).

The results for PC/ABS 60:40 show a dramatic increase in wear volume, in comparison to the reference condition, reaching values many orders of magnitude higher than the correspondent test for R3 x R3. Given the much lower hardness and weaker structure of the polymer, this was expected. When plotting the results in a similar manner to what was done for the reference condition, the wear rates for this polymer blend can be analyzed. This is shown in Fig. 4.6.

Since these marks showed remarkable circular shapes, the evolution of the scars' depths was also analyzed. A graphical representation of this depth with increasing number of cycles is shown in Fig. 4.7.

A few conclusions can be withdrawn from the dispersion of data shown in this figure. Namely,

- With the same definition of wear rate as done for the reference condition, the wear rate for PC/ABS at 2.0 kN ($\approx 22.63\mu\text{m}^3/\text{kilocycle}$) is more than 10 times higher than at 1.0 kN ($\approx 1.68\mu\text{m}^3/\text{kilocycle}$);
- Comparing the wear rate increase from 1.0 kN to 2.0 kN for R3 ($\approx 2x$) and PC/ABS 60:40 ($\approx 13x$), it can be concluded that PC/ABS is more than 6 times more sensible

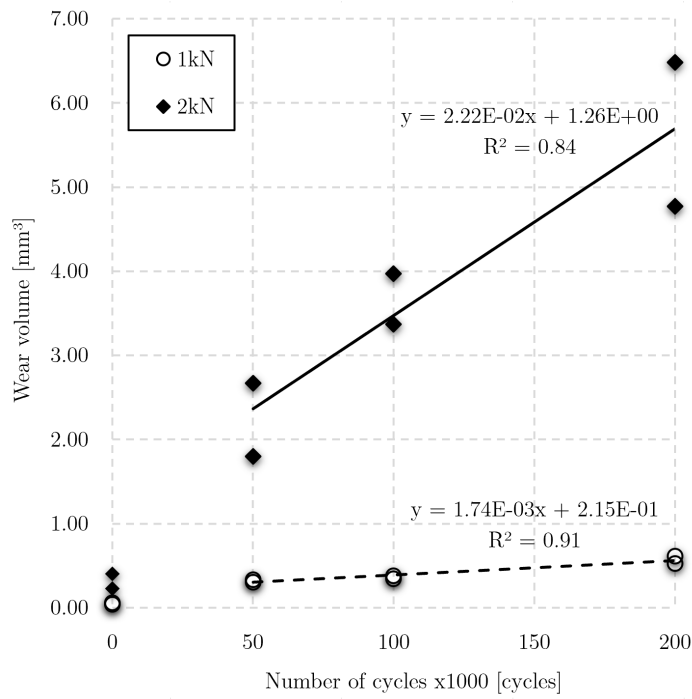


Figure 4.6: Net wear volume versus number of cycles: PC/ABS 60:40 flat counterpart.

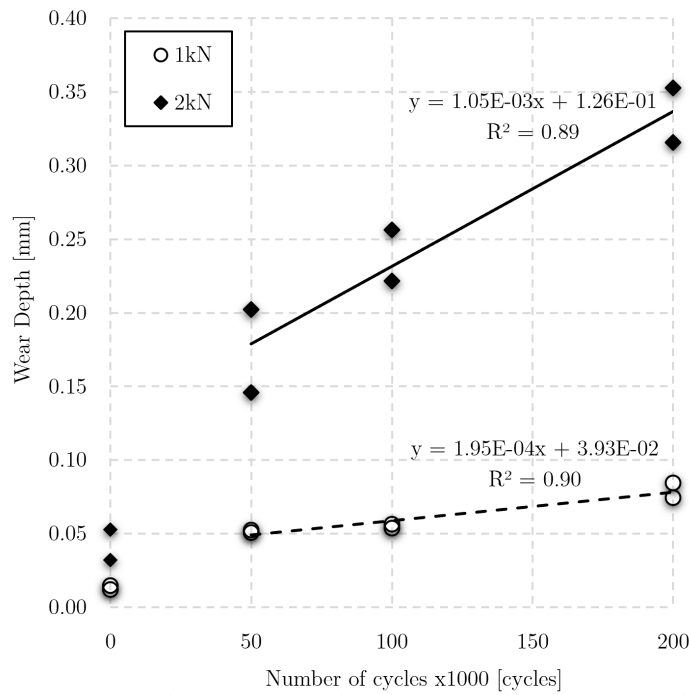


Figure 4.7: Wear depth versus number of cycles: PC/ABS 60:40 flat counterpart.

to load variations;

- Analyzing Fig. 4.7, one can promptly see the linear relationship of the wear depth with the number of cycles. In other words, increasing wear cycles do not only increase the scars' diameter, but also its depth in a regular manner.
- Perhaps the most important conclusion is that, as seen in Fig. 4.6, the evolution of worn volume for PC/ABS 60:40 is highly linear. Indeed, the R-squared values for linear regression of data are very high for both load levels, namely, 0.84 for 1.0 kN and 0.91 for 2.0 kN. This is of extreme importance for the research, as will be pointed out in Sec. 4.4,

4.4 Life Estimations

According to standardized guidelines for failure analysis of mooring chains [58], one of the failure criteria is that the superficial defects' dimensions must not exceed 5% of the component's nominal diameter.

Therefore, considering a common offshore chain link with 120 mm diameter, for instance, any defects on its surface should have dimensions lower than 6 mm. Assuming those defects to be perfect hemispherical wear marks, they should have a radius lower than 3 mm and volume up to $56mm^3$. Based on the results shown in Sec. 4.3, a link would show, after 200 kcycles, scars far smaller than the maximum threshold. Namely, for 1.0 kN, the scar would have $0.04mm^3$, representing 0.07% of the established tolerance, and for 2.0 kN, it would show a mark with $0.09mm^3$, corresponding to 0.16% of the limit value. Therefore, a chain link would withstand 285.7 M wear cycles before being replaced or repaired. Evidently, this is the best-case scenario, i.e., a one-sided linearly evolving wear behavior at a constant load. In practical applications, given the highly non-linear behavior of wear in R3 x R3 contacts, this problem is tackled by costly and complicated maintenance.

The main purpose of this work is to evaluate and determine whether PC/ABS 60:40 is a suitable material for extending the life of mooring chain links by being used to coat those elements. Considering that the linear relationship seen in Fig. 4.6 would be sustained indefinitely (and it should be noted that there is no reason to think otherwise), it can be estimated that a 5 mm thick coating of PC/ABS 60:40 to R3 offshore mooring chain links would extend the lifetime of those components by 25.4 M cycles, at 1.0 kN and by 4.6 M cycles at 2.0 kN. In other words, those are the number of cycles needed to completely remove a 5 mm coating of this polymer.

One might argue that, because wear rates for PC/ABS are much larger than for R3 steel, it would make no sense to coat a link with this material. However, given the linear evolution of wear under torsional fretting conditions, observed in this study, one can safely say that this coating approach has great potential to be employed in practical applications. That

is because, aside from actually extending the lifetime of the link in millions of cycles per millimeter of coating, the high predictability of PC/ABS' behavior is a determinant factor to designers and maintenance engineers, since it provides a much more reliable method of protecting the mooring chain systems and immensely reduces costs associated with production stoppage or corrective procedures of unexpected failures.

Chapter 5

Conclusions

This work presented experimental data regarding the torsional fretting wear behavior of two material pairings, namely, R3 offshore steel against PC/ABS 60:40 and R3 against R3, in a sphere-to-flat configuration. The specimens used were cylindrical R3 tools with hemispherical tips and flat prismatic samples of both R3 and PC/ABS. Torsional fretting wear tests were done, so as to emulate conditions experienced by chain links in mooring systems of Floating Production Storage and Off-loading (FPSO) vessels. Load levels of 1.0 kN and 2.0 kN were used in the tests with 0, 50, 100 and 200 wear kilocycles of $\pm 1.0^\circ$ range with a 5 Hz oscillation frequency.

The objective of this work was to determine whether this specific polymer blend, namely, PC/ABS 60:40 is a suitable candidate for coating a mooring chain steel link, so as to extend its lifetime.

Four main aspects were studied, namely: morphology of the wear scars, hardness of the materials, wear evolution for each pairing and life estimations.

The main conclusions withdrawn from this study are as follows:

- R3 steel is clearly much harder than PC/ABS 60:40, as expected. However, it was observed that an unpredictable and highly non-linear behavior occurred in R3 x R3 configuration, due to a complex material exchange in the contact interface. With increasing loads and number of cycles, this phenomenon became even more critical, requiring a refined and time consuming analysis for evaluating the wear volume;
- Direct relations between wear volume, number of cycles and applied loads were observed in all conditions tested. The difference being that, for R3 x R3, this relationship is initially fairly non-linear (during the running-in phase, which lasted less than 50k cycles), whereas for R3 x PC/ABS 60:40 it is quite linear and predictable even considering the unstable initial phase of the wear phenomenon;
- The scratch marks found for both configurations are rather interesting, and desire a thorough analysis, as shown in Sec. 4.2;

- Both configurations, namely, R3 x R3 and R3 x PC/ABS showed two distinct zones, as expected: a central adhesion zone and an outer annular mixed-slip region. The areas of those zones seemed to be proportional to the applied load. However, PC/ABS samples showed remarkably circular contact zones, whose surfaces seemed to get smoother with increasing load and number of cycles. Whereas R3 samples exhibited irregularly shaped marks, with a rather interesting chipping pattern in the adhesion zone, probably due to the debris dynamics in this region, as explained in Sec. 4.2.
- Results showed a highly predictable behavior of wear on PC/ABS 60:40, meaning that it could possibly be used to coat a chain link and safely protect it against wear for millions of cycle per millimeter of coating. This predictability is an essential characteristic of coating materials and must be highlighted.
- Finally, a simple and straightforward estimation of lifetime extension for a mooring chain link with a PC/ABS 60:40 coating can be done, given its linear relation between wear depth and number of cycles.

Therefore, it can be concluded that PC/ABS 60:40 is indeed a suitable and rather promising candidate for coating steel chain links used in mooring chain systems, possibly being able to dramatically reduce costs with unexpected failures and periodic maintenance.

Even though the findings of this work are already interesting and relevant from an economical standpoint, further research is needed. Similar tests with various polymer blends and even with PC/ABS of different weight ratios should demonstrate which material would be optimal for the proposed applications.

REFERENCES

- [1] YAGHIN, A.; MELCHERS, R. Long-term inter-link wear of model mooring chains. *Marine Structures*, v. 44, p. 61–84, 2015.
- [2] BARTZ, W. History of tribology – the bridge between the classical antiquity and the 21st century. In: . [S.l.: s.n.].
- [3] POPOV, V. L. *Contact Mechanics and Friction: Physical Principles and Applications*. [S.l.]: Springer-Verlag Berling Heidelberg.
- [4] JOHNSON, K. L. *Contact Mechanics*. [S.l.]: Cambridge University Press.
- [5] BHUSHAN, B. *Modern Tribology Handbook*. [S.l.]: CRC Press, 2001. (The mechanics and materials science series, v. 1). ISBN 9780849384035.
- [6] ZHU, M. H.; ZHOU, Z. R. On the mechanisms of various fretting wear modes. *Tribology International*, v. 44, p. 1378–1388, 2011.
- [7] LINS, G. F.; AMARAL, T. L.; DOCA, T. Design and manufacture of a sample holder device for fretting wear tests. In: COBEM. Uberlândia, 2019.
- [8] GORDON, R.; MG, B.; ALLEN, E. Mooring integrity management: a state-of-the-art review. *Proceedings of the Offshore Technology Conference, Houston, Texas, OTC 25134*, 2014.
- [9] BJØRNSSEN, E. *Chains in Mooring Systems*. 2014.
- [10] MA, K. Historical review on integrity issues of permanent mooring systems. In: OFFSHORE TECHNOLOGY CONFERENCE. [S.l.], 2013.
- [11] MA, K. et al. A historical review on integrity issues of permanent mooring systems. *Offshore Technology Conference*. <https://www.onepetro.org/conference-paper/OTC-24025-MS>.
- [12] PAUW, J. D. et al. A full scale test rig for assessment of abrasive wear of shackle chains. *Wear*, v. 302, p. 1017–1025, 2013.
- [13] FALTINSEN, O. M. *Sea Loads on Ships and Offshore Structures*. [S.l.]: Cambridge University Press, 1990.

- [14] AMERICAN BUREAU OF SHIPPING. *Guide for Positioning Mooring Systems*. [S.l.], 2018.
- [15] WATERHOUSE, R. B. Fretting wear. *Wear*, v. 100, p. 107–118, 1984.
- [16] DUGGAL, A.; W., F. Anchor leg system integrity - from design through service life. *Offshore Technology Conference*, 2010. P. 1-15.
- [17] DNV. *OFFSHORE STANDARD DNV-OS-E302: OFFSHORE MOORING CHAIN*. [S.l.].
- [18] RIDGE, I.; HOBBS, R.; FERNANDEZ, J. Predicting the torsional response of large mooring chains. *Offshore Technology Conference*, 2006. P. 1-13.
- [19] TAKAYAMA, T.; TOKUBUCHI, K. Economical design of elastic chain for mooring through the numerical simulation. *International Society of Offshore and Polar Engineers*. <https://www.onepetro.org/conference-paper/ISOPE-I-02-168>.
- [20] BROWN, D. T.; MAVRAKOS, S. Comparative study on mooring line dynamic loading. *Marine Structures*, v. 12, p. 131–151, 1999.
- [21] HUND, J.; NAUMANN, J.; SEELIG, T. An experimental and constitutive modeling study on the large strain deformation and fracture behavior of pc/abs blends. *Mechanics of Materials*, v. 124, p. 132–142, 2018.
- [22] ISHIKAWA, M. Stability of plastic deformation and toughness of polycarbonate blended with poly(acrylonitrile-butadiene-styrene) copolymer. *Polymer*, v. 36, n. 11, p. 2203–2210, 1994.
- [23] WIN, K. N.; LIU, E. Thermal, mechanical and tribological properties of polycarbonate/acrylonitrile-butadiene-styrene blends. *Journal of Polymer Engineering*, v. 33, p. 535–543, 2013.
- [24] KRACHE, R.; DEBBAH, I. Some mechanical and thermal properties of pc/abs blends. *Materials Sciences and Applications*, v. 2, p. 404–410, 2011.
- [25] UTRACKI, L. *Commercial Polymer Blends*. [S.l.]: Springer-Science+Business Media B.V.
- [26] MENS, J. W. M.; GEE, A. W. J. de. Friction and wear behaviour of 18 polymers in contact with steel in environments of air and water. *Wear*, v. 149, p. 255–268, 1991.
- [27] ZAITSCV, A. L. Mechanisms of hard alloy wear in frictional processes with polymers and composite materials. *Wear*, v. 162, p. 40–46, 1993.
- [28] LEMM, J. et al. The influence of surface hardness on the fretting wear of steel pairs — its role in debris retention in the contact. *Tribology International*, v. 81, p. 258–266, 2015.

- [29] KIRK, A. M. et al. The effect of frequency on both the debris and the development of the tribologically transformed structure during fretting wear of a high strength steel. *Wear*, v. 426–427, p. 694–703, 2019.
- [30] WARMUTH, A. R. et al. The effect of contact geometry on fretting wear rates and mechanisms for a high strength steel. *Wear*, v. 301, p. 491–500, 2013.
- [31] ZHANG, P. et al. Torsional fretting and torsional sliding wear behaviors of conical against 42crmo4 under dry condition. *Tribology International*, v. 118, p. 11–19, 2018.
- [32] ZEGATTI, M. *ESTUDO DA INFLUÊNCIA DO DESGASTE NA FALHA PREMATURA DE COMPONENTES DE LINHAS DE ANCORAGEM*. 2016.
- [33] JOST, P. H. *Lubrication (Tribology) Education and Research. A Report on the Present Position and Industry's Need*. [S.l.], 1966.
- [34] MYSHKIN, N.; GORYACHEVA, I. Tribology: Trends in the half-century development. *Journal of Friction and Wear*, v. 37, n. 6, p. 513–516, 2016.
- [35] HOLMBERG, K.; ANDERSSON, P.; ERDEMIR, A. Global energyconsumption-duetofrictioninpassengercars. *Tribology International*, v. 47, p. 221–234, 2012.
- [36] HUTCHINGS, I. M. Leonardo da vinci's studies of friction. *Wear*, v. 360–361, p. 51–66, 2016.
- [37] VINCI, L. *Tratado de Estática Y Mecánica en Italiano*. [S.l.]: McGraw Hill.
- [38] POPOVA, E.; POPOV, V. The research work of coulomb and amontons and generalized friction laws. *Friction*, v. 3, p. 183–190, 2015.
- [39] GILLMOR, C. S. *Coulomb and the Evolution of Physics and Engineering in Eighteenth-Century France*. [S.l.]: Princeton University Press.
- [40] POPOV, V. L. et al. On the role of scales in contact mechanics and friction between elastomers and randomly rough self-affine surfaces. *Scientific Reports*, v. 5, 2015.
- [41] HUTCHINGS, I.; SHIPWAY, P. *Friction and Wear of Engineering Materials*. [S.l.]: Butterworth-Heinemann.
- [42] HERTZ, H. Über die berührung fester elastischer körper. *J. reine und angewandte Mathematik*, v. 92, p. 156–171, 1822.
- [43] HERTZ, H. Über die berührung fester elastischer körper und über die harte. *Verhandlungen des Vereins zur Beförderung des Gewerbefleisses*, 1822.
- [44] ZMITROWICZ, A. Wear patterns and laws of wear - a review. *journal of Theoretical and Applied Mechanics*, v. 44, p. 219–253, 2006.

- [45] LUDEMA, K. C. *Friction, Wear, Lubrication*. [S.l.]: CRC Press.
- [46] ARCHARD, J. F. Contact and rubbing of flat surfaces. *Journal of Applied Physics*, v. 24, p. 981–988, 1953.
- [47] IMECHE. Proceedings of the conference on lubrication and wear. In: . London, 1957.
- [48] RABINOWICZ, E. *Wear coefficients - metals*. [S.l.]: ASME, 1980. (Wear control handbook, v. 1).
- [49] EVANS, A. G.; MARSHALL, D. B. *Wear mechanism in ceramics*. [S.l.]: ASME, 1981. (Fundamentals of Friction and Wear of Materials, v. 1).
- [50] CHALLEN, J. M.; OXLEY, P. L. B.; HOCKENHULL, B. S. Prediction of archard's wear coefficient for metallic sliding friction assuming a low cycle fatigue wear mechanism. *Wear*, v. 111, p. 275–288, 1986.
- [51] QUINN, T. F. J. Wear and lubrication. In: INTERNATIONAL CONFERENCE ON TRIBOLOGY-FRICTION, INSTITUTE OF MECHANICAL ENGINEERS. 253–259, 1987.
- [52] SARKAR, A. D. *Materials Science and Technology. Vol 18: Wear of Metals*. [S.l.]: Pergamon Press, 1987.
- [53] GEE, M. et al. Results from an interlaboratory exercise to validate the micro-scale abrasion test. *Wear*, v. 259, p. 27–35, 2005.
- [54] STEIER, V.; PIRES, M.; DOCA, T. The influence of diamond-like carbon and anodised aluminium oxide coatings on the surface properties of the sae 305 aluminium alloy. *Journal of the Brazilian Society of Mechanical Sciences and Engineering*, v. 40:41, 2018.
- [55] GRELLMANN, W.; SEIDLER, S. *Landolt-Börnstein Numerical Data and Functional Relationships in Science and Technology, vol. 6A*. [S.l.]: Springer-Verlag, 2014.
- [56] WANG, S. Torsional wear behavior of monomer casting nylon composites reinforced with gf: Effect of content of glass fiber. *Tribology Transactions*, v. 56:2, p. 178–186, 2013.
- [57] CRUZADO, A. et al. Fretting wear of thin steel wires. part 1: Influence of contact pressure. *Wear*, v. 11–12, p. 1409–1416, 2010.
- [58] AMERICAN BUREAU OF SHIPPING. *Guide for the Certification of Offshore Mooring Chain*. [S.l.], 2017.

Appendix I

Torsional fretting wear test procedures - MTS 809 and sample holder

The following is a procedural algorithm for performing a torsional fretting wear tests using a sample holder (see Chapter 3 for more details) and an axial-torsional testing system (MTS 809).

Disclaimer: It should be noted that this proposed method might not be the optimal way to perform such tests and the following should be regarded as a guideline, not a mandatory procedure. Nevertheless, it has been proved that the proposed method is a consistent and robust method to perform torsional fretting wear tests under the effects of inelastic strains.

First Part: Monotonic Compression Test

1. With the computer turned on (check login information with the technician), launch *Station Manager* software;
2. Select the following configuration "*célula 25kN 110Nm*" and check *Exclusive Control*;
3. Turn on the hydraulic pumps as follows: first turn on HPU-J25 (in two stages) and then turn on the manifold (lower button on the screen);
4. Reset all *Interlocks*;
5. Set up a *Program Interlock* for load so the specimens can be safely placed in the machine;
6. Set up the testing machine:
 - (a) Make sure the collet's diameter is 15 mm;
 - (b) Place the holding device (with the prismatic shaped already locked in place) inside the lower grip without touching the bottom of the grip;
 - (c) Place the cylindrical tool inside the upper grip, so that the hemispherical tip is pointing down. Obs.: hold the tool with a cloth so the tip is not contaminated and make sure not to hit the top of the grip;

Table 5.1: Examples of limits set up on the Limit Detector.

Limit Detector	Upper Limit	Upper Action	Lower Limit	Lower Action
Axial Displacement	(*)	C-Stop	(*)	C-Stop
Axial Force	P(†)	Program Interlock	-P(†)	Program Interlock
Torsional Angle	6.00°	C-Stop	6.00°	C-Stop
Torsional Torque	20.0Nm	C-Stop	-20.0Nm	C-Stop

(*) Relative to the initial specimen's position.
(†) P, represents the desired compressive force [kN].

- (d) Set the hydraulic pressure on the machine's bench to around 4.0 kpsi;
- (e) Switch the speed mode to slow (that is the button with a turtle on it);
7. Make sure the lower and upper grips have a large distance between them;
8. Go to *Manual Command* -> *Axial Displacement* and set it to 0.0 mm;
9. Manually lower the upper bar of the machine so that the tool is about 1 mm away from the top of the holding device
10. Go to *Station Manager* and set up the test itself:
 - (a) Go to *Displacement Control* -> *Rate* and type 0.5 mm/min;
 - (b) Go to *End level type* -> *Relative* and set it up to 5.0 mm (which is the sample's thickness);
 - (c) Go to *Data Acquisition* -> *Timed* -> *Sample Rate* and set it up to 10 Hz;
 - (d) Still on *Data Acquisition*, include *Axial Displacement*, *Axial Force*, *Torsional Angle* and *Torsional Torque*;
 - (e) Moreover, make sure to specify all other information needed for your file, i.e., file name, file extension, etc. This can all be done inside the *Test Setup* environment;
11. On *Limit Detectors*, set up the limits desired. An example is given on Tab. 5.1
12. IMPORTANT: Remember to check the directions of the axis built in the system machine. Namely, in this particular system, the positive direction of the z-axis is pointed downwards. In other words, if the lower is grip is at the origin (0.00 mm), and one wants to move it 2.00mm up, they should displace it to -2.00 mm.;
13. Gradually move the lower grip upwards through the *Manual Command* interface on *Station Manager*, so that the specimen gets to about 0.5 mm away from the tool's tip;
14. At this moment, off-set the relative distance, so that it starts to be counted from this point on.;
15. Run the test

16. After the desired load, P, is reached, the test stops automatically and the data file should be found in the directory specified by the user.

Second Part: Cyclic Torsional Wear Test

1. Launch MPE;
2. Open any test file saved on the research's folder (feel free to contact the author if files are not found);
3. Go to block diagram tab;
4. Check the *Dwell Force* block and make sure the value input is the desired load;
5. Check the *Cyclic* block and make sure that, under the *Limit Detection* options:
6. *Axial Force*: desired values for safety stoppage;
7. *Torsional Angle*: -1.00° to 1.00° ;
8. *Frequency*: 5 Hz;
9. *Cycles*: desired number of cycles. The values used for this research were 50, 100 and 200 kcycles;
10. Check the *Data Acquisition* block and make sure the acquisition frequency is set to 10 Hz;
11. Go to *Test-Run Display* and custom-change each plot for the specific test being run, so that parameters such as torsional torque, normal load and other can be easily monitored by the user. It is suggested to change the trace time to .25 s in *Run-mode: Program Control -> Trace time*;
12. Go to *Test Runs -> New Test Run -> geometry* and select *generic*;
13. Return to *Station Manager*, go to *Limit Detectors* and change the limits to values higher than those inside MPE, so that they function as a second layer of safety;
14. Run the test on MPE;
15. When the test is over, go to *Test-Run -> Export Raw Data* and save files both as .csv and .txt;
16. Go back to *Station Manager*, enable *Manual Command* and lower the normal load gradually until it reaches 0.0 N;
17. Turn off the manifold (lower pump button inside *Station Manager*) and then the other pump, in two steps;

18. Disassemble the test, carefully extracting the tool and the sample without touching the contact areas;
19. Catalog the tool/sample pair and store them appropriately in separate zip-lock bags;
20. Turn off the hydraulic pumps in the following order: first the lower one (manifold), then the upper one in three stages
21. Close the MPE and the Station manager software. Shut down the computer.